JOURNAL OF PETROLOGY | VOLUME 46 | NUMBER 5 | PAGE 893–919 | 2005 | doi:10.1093/petrology/egi004

Formation, Crystallization, and Migration of Melt in the Mid-orogenic Crust: Muskoka Domain Migmatites, Grenville Province, Ontario

T. SLAGSTAD*, R. A. JAMIESON AND N. G. CULSHAW

DEPARTMENT OF EARTH SCIENCES, DALHOUSIE UNIVERSITY, HALIFAX, N.S., CANADA, B3H 3J5

RECEIVED APRIL 30, 2004; ACCEPTED DECEMBER 1, 2004
ADVANCE ACCESS PUBLICATION JANUARY 21, 2005

Migmatitic orthogneisses in the Muskoka domain, southwestern Grenville Province, Ontario, formed during the Ottawan stage (c. 1080–1050 Ma) of the Grenvillian orogeny. Stromatic migmatites are volumetrically dominant, comprising granodioritic gneisses with 2–5 cm thick granitic leucosomes, locally rimmed by thin melanosomes, that constitute 20–30 vol. %, and locally 40–50 vol. %, of the outcrops. Patch migmatites in dioritic gneisses form large (>10 m) pinch-and-swell structures within the stromatic migmatites, and consist of decimetre-scale, irregular patches of granitic leucosome, surrounded by medium-grained hornblende–plagioclase melanosomes interpreted as restite. The patches connect to larger networks of zoned pegmatite dykes. Petrographic and geochemical evidence suggests that the patch leucosomes formed by 20–40% fluid-present, equilibrium melting of the dioritic gneiss, followed by feldspar-dominated crystallization. The dyke networks may have resulted from hydraulic fracturing, probably when the melts reached water saturation during crystallization. Field and geochemical data from the stromatic migmatites suggest a similar petrogenesis to the patch migmatites, but with significant additions of externally derived melts, indicating that they acted as conduits for melts derived from deeper structural levels within the orogen. We hypothesize that the Muskoka domain represents a transfer zone for melts migrating to higher structural levels during Grenvillian deformation.

KEY WORDS: *migmatite geochemistry; partial melting; melt crystallization; melt transport; Grenville orogen*

INTRODUCTION

Partial melting in the middle to lower crust may take place in response to dehydration of hydrous minerals such as muscovite, biotite, and amphibole (e.g. Thompson, 1982; Nédélec *et al.*, 1993) or influx of externally derived hydrous fluids (e.g. Brown, 1979; Montel *et al.*, 1992). In many cases, geochemical evidence suggests that the melts may undergo magmatic differentiation, either *in situ* or while migrating from the site of melting (e.g. Sawyer, 1987; Sawyer *et al.*, 1999). Most migmatites form in regions of orogenically thickened crust and a number of field and experimental studies have indicated a significant potential for melt migration during deformation (e.g. Collins & Sawyer, 1996; Brown & Solar, 1998; Sawyer *et al.*, 1999; Barraud *et al.*, 2004). Partial melting and melt migration are important in the compositional differentiation of the continental crust (e.g. Fyfe, 1973; Vielzeuf *et al.*, 1990) and may influence orogenic evolution by lowering crustal strength (e.g. Hollister & Crawford, 1986; Davidson *et al.*, 1994; Beaumont *et al.*, 2001; Jamieson *et al.*, 2002). Understanding how melts form, evolve, and move during orogenesis is therefore fundamental for understanding the geochemical structure of the continental crust (e.g. Sandiford & McLaren, 2002), the formation of middle to shallow crustal granitoid plutons and batholiths (e.g. Collins & Sawyer, 1996; Solar & Brown, 2001), and structural evolution during orogenesis (e.g. Hollister, 1993; Beaumont *et al.*, 2004).

The Muskoka domain in the Central Gneiss Belt, SW Grenville Province, Ontario (Fig. 1), is characterized by leucosome-rich migmatitic orthogneisses (Timmermann *et al.*, 2002; Slagstad, 2003) that formed at mid-crustal levels at the peak of Grenvillian (Ottawan) contractional deformation and high-grade metamorphism

*Corresponding author. Present address: Geological Survey of Norway (NGU), Leiv Erikssons v. 39, 7491 Trondheim, Norway. Telephone: +47 73 90 42 29. Fax: +47 73 92 16 20.
E-mail: Trond.Slagstad@ngu.no

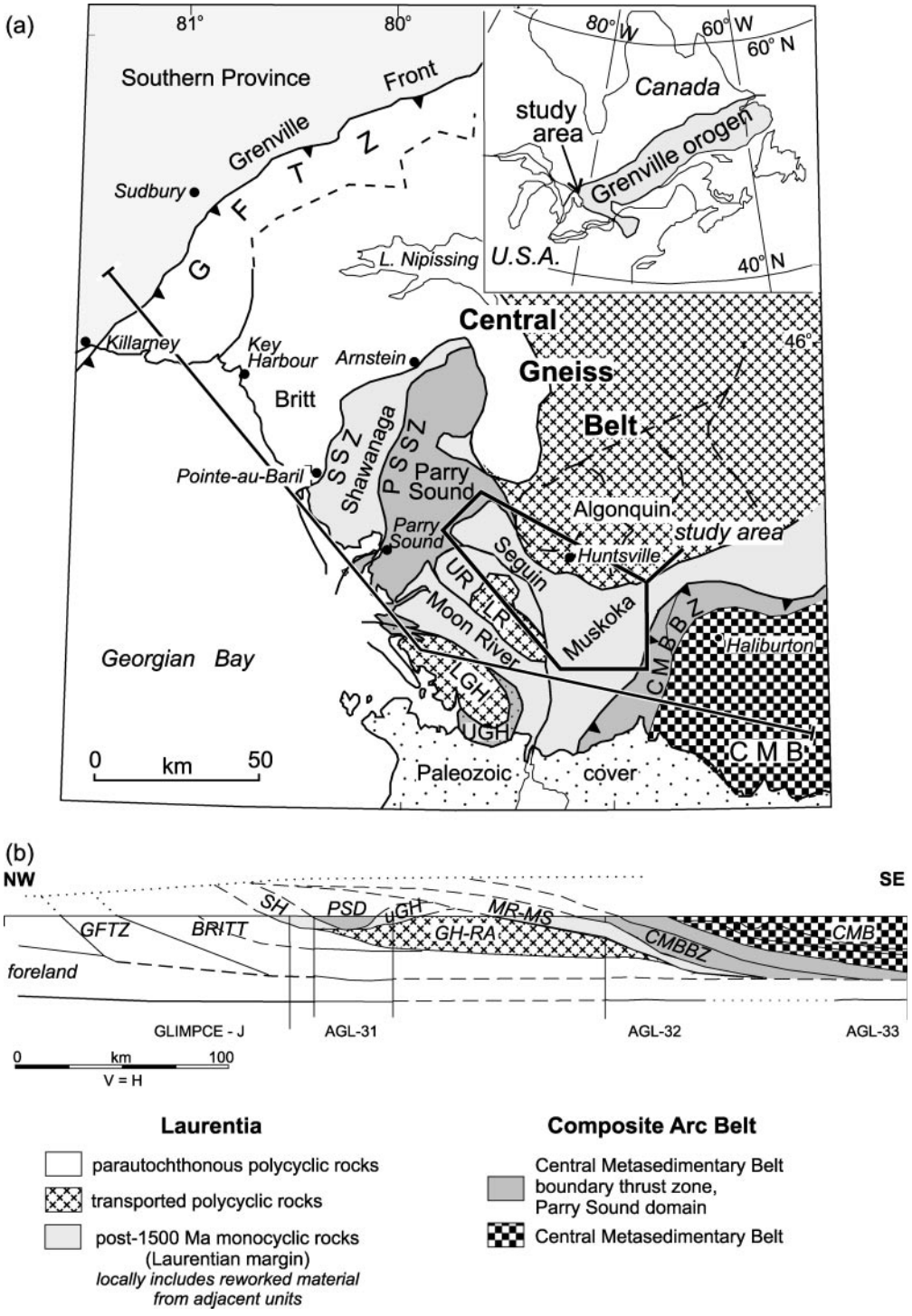

Fig. 1. (a) Location and geology of the study area. Bold barbed lines indicate major thrust boundaries and bold non-barbed lines indicate other important structural contacts. Fine lines represent domain boundaries after Davidson (1984) and Davidson & van Breemen (1988), with minor modifications by Culshaw *et al.* (1997). (b) Crustal-scale cross-section from the Grenville Front to the Central Metasedimentary Belt, modified after Culshaw *et al.* (1997); based on geological and structural data, discussed by Culshaw *et al.* (1997), and seismic reflection profiles AGL-31, 32, 33 and GLIMPCE-J (Green *et al.*, 1988; White *et al.*, 1994). Composite Arc Belt defined by Carr *et al.* (2000). GFTZ, Grenville Front Tectonic Zone; SSZ, Shawanaga Shear Zone; PSSZ, Parry Sound Shear Zone; UR, Upper Rosseau domain; LR, Lower Rosseau domain; UGH, Upper Go Home domain; LGH, Lower Go Home domain; CMBBZ, Central Metasedimentary Belt boundary thrust zone; CMB, Central Metasedimentary Belt; PSD, Parry Sound domain. In cross-section: SH, Shawanaga domain; MR-MS, Moon River–Muskoka domains; GH-RA, Go Home–Rosseau domains.

(Timmermann *et al.*, 1997; Slagstad *et al.*, 2004*b*). The Muskoka domain, therefore, presents a natural laboratory in which the effects of partial melting in the middle orogenic crust can be studied. Despite several recent studies (Timmermann, 1998; McMullen, 1999; Timmermann *et al.*, 2002), a number of questions regarding the petrogenesis of these rocks remain. Unresolved problems include the role of fluid during partial melting (e.g. Timmermann, 1998; Timmermann *et al.*, 2002), whether the abundant leucosomes represent *in situ* or externally derived melts, the extent to which leucosome compositions were modified by fractionation, and the possible relationships between melting, melt migration, and orogenic evolution. The purpose of this paper is to present field, petrographic, and geochemical data from the Muskoka domain migmatites in an attempt to answer these questions, and thereby contribute to a better understanding of the causes and consequences of partial melting in the Grenville orogen and, by analogy, other large collisional orogens.

GEOLOGICAL SETTING

The Central Gneiss Belt (Wynne-Edwards, 1972) of the Grenville Province, Ontario, exposes large tracts of upper amphibolite- to granulite-facies migmatitic gneisses of dominantly Laurentian affinity, formed by continent–arc(s) and/or continent–continent collision(s) along the southeastern margin of Laurentia between 1200 and 1000 Ma (e.g. Rivers, 1997; Carr *et al.*, 2000). In Ontario (Fig. 1), the Central Gneiss Belt comprises pre-1350 Ma high-grade gneisses, formed along the active southeastern margin of the pre-Grenvillian Laurentian craton (Culshaw & Dostal, 1997; Rivers, 1997; Rivers & Corrigan, 2000; Culshaw & Dostal, 2002; Slagstad *et al.*, 2004*a*), and assembled during multiple stages of NW-directed convergence (Culshaw *et al.*, 1997). The earliest stage of convergence, termed the 'Elzevirian orogeny' (*c.* 1200–1160 Ma; Moore & Thompson, 1980), involved assembly of arc terranes offshore from, or at the distal southeastern edge of, Laurentia (e.g. Carr *et al.*, 2000). In the study area, the main collisional event, termed the 'Ottawan orogeny' (Moore & Thompson, 1980), began some time after 1120 Ma and resulted in emplacement of post-1400 Ma arc and back-arc assemblages of the Central Metasedimentary Belt over the Central Gneiss Belt along a crustal-scale shear zone termed the Central Metasedimentary Belt boundary thrust zone (Hanmer & McEachern, 1992). The Ottawan orogeny was associated with foreland-propagating convergence and widespread upper amphibolite- to granulite-facies metamorphism and partial melting at 1085–1035 Ma (e.g. Culshaw *et al.*, 1997; Timmermann *et al.*, 1997; McMullen, 1999; Carr *et al.*, 2000; Wodicka *et al.*, 2000; Slagstad, 2003). This orogenic phase was followed by regionally significant ductile extension at *c.* 1020 Ma (Ketchum *et al.*, 1998), and there is evidence for both earlier and later extensional deformation in some parts of the region (van der Pluijm & Carlson, 1989; Timmermann *et al.*, 2002). A final stage of orogen-wide convergence affected the Grenville Front Tectonic Zone at *c.* 1000 Ma (e.g. Haggart *et al.*, 1993; Krogh, 1994).

STUDY AREA

The Muskoka domain constitutes the uppermost structural level of the Central Gneiss Belt (Culshaw *et al.*, 1983), in the immediate footwall to the Central Metasedimentary Belt boundary thrust zone (Figs 1 and 2). East- to SE-dipping, grey migmatitic orthogneisses with protolith compositions ranging from gabbro to granite, with granodiorite predominant (Timmermann, 1998; Slagstad *et al.*, 2004*a*), and major and trace element compositions suggest formation in a continental magmatic arc (McMullen, 1999; Slagstad *et al.*, 2004*a*). Radiometric (U–Pb zircon) ages from the grey gneisses range from *c.* 1480 to 1430 Ma, but most fall in a narrow range between *c.* 1450 and 1460 Ma (Timmermann *et al.*, 1997; Nadeau & van Breemen, 1998; McMullen, 1999). The Muskoka domain is bounded above by the Central Metasedimentary Belt boundary thrust zone, which contains evidence of thrusting between *c.* 1080 and 1050 Ma (van Breemen & Hanmer, 1986; McEachern & van Breemen, 1993; Burr & Carr, 1994). Adjacent to the Muskoka domain, the Central Metasedimentary Belt boundary thrust zone includes reworked migmatites similar to those in its immediate footwall. Peak metamorphic conditions of 750–850°C at 0·9–1·15 GPa (Fig. 3) were attained at *c.* 1080–1060 Ma (Timmermann, 1998; Timmermann *et al.*, 2002; S. Gagné & J. Hawken, unpublished data, 2002). Timmermann *et al.* (1997) dated a foliation-parallel leucosome in the Muskoka domain at 1064 ± 18 Ma (U–Pb zircon, TIMS), and this age has recently been corroborated by sensitive high-resolution ion microprobe (SHRIMP) dating (1067 ± 9 Ma; Slagstad *et al.*, 2004*b*).

MUSKOKA MIGMATITES

We distinguish between two types of migmatite, referred to as stromatic and patch migmatite, based on leucosome morphology and type of host rock. The stromatic migmatites typically have light grey, quartz monzodioritic to granodioritic mesosomes, and are by far the dominant type of migmatite in the Muskoka domain. The patch migmatites have dioritic mesosomes, and are typically found as outcrop-scale bodies within the stromatic migmatites. Because of their generally lower strain, these rocks provide some constraints on melt generation and

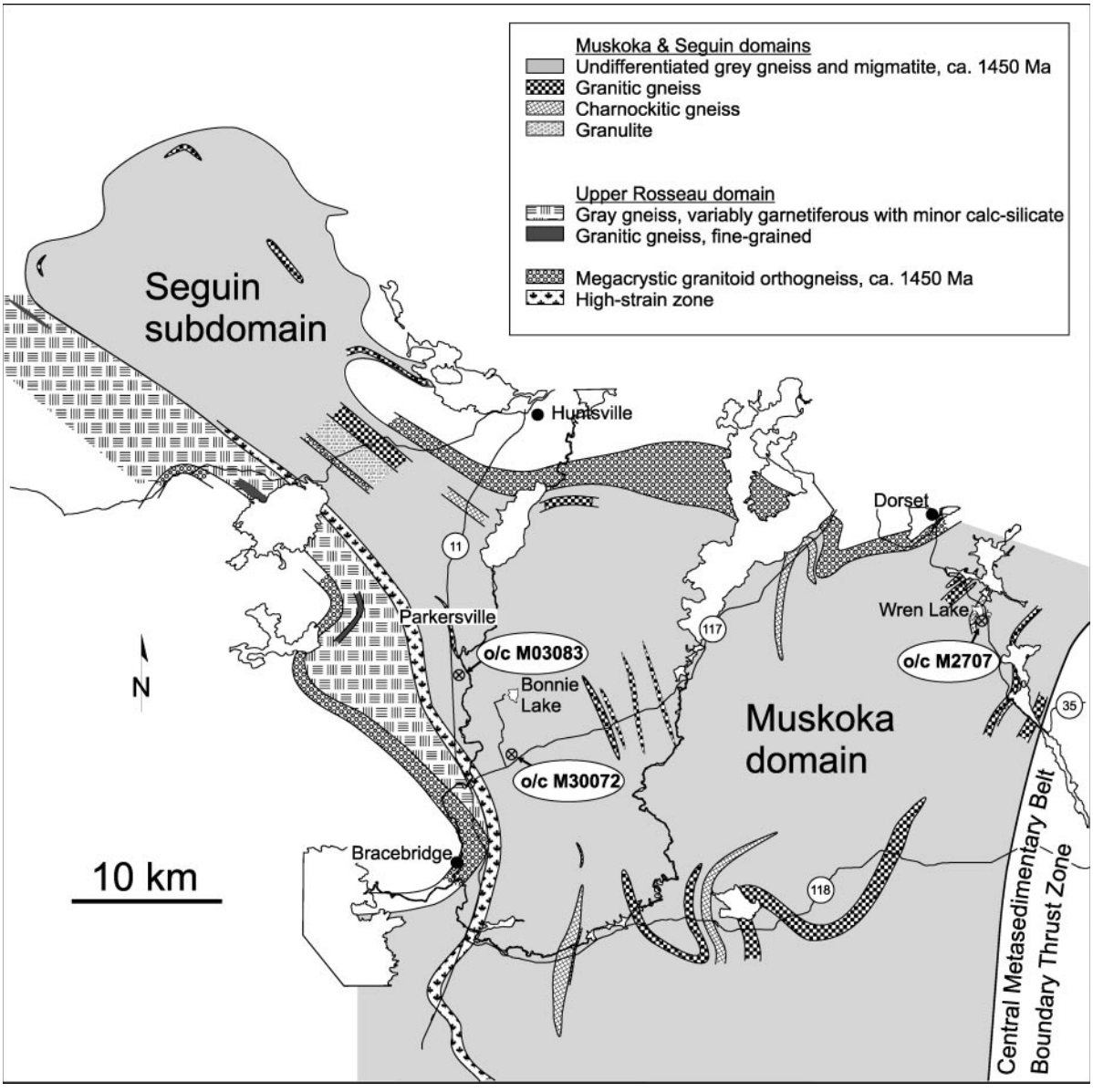

Fig. 2. Geological map of the Muskoka domain showing dominant lithological units and the locations of the investigated outcrops. UTM coordinates (UTM zone 17) of the investigated outcrops: o/c M03083 (Parkersville): 5002 400N, 632 700E; o/c M30072 (Bonnie Lake): 4995 500N, 636 500E; o/c M2707 (Wren Lake): 5005 430N, 668 550E.

transport processes indeterminable from the stromatic migmatites.

Three representative outcrops were investigated in detail (Fig. 2). The first two outcrops are located south of Parkersville (o/c M03083) and Bonnie Lake (o/c M30072), in the western part of the Muskoka domain, and display stromatic and patch migmatites, respectively. The third outcrop is located at Wren Lake (o/c M2707), in the eastern part of the Muskoka domain, and comprises both stromatic and patch migmatites separated by sharp, foliation-parallel contacts. Most of the investigated migmatites preserve pre-migmatization compositional banding and foliation and can be classified as metatexite (Brown, 1973). The terms 'leucosome', 'mesosome', and 'melanosome' are used below as defined by Ashworth (1985).

Patch migmatites

The patch migmatites are morphologically more varied than the stromatic migmatites and range from small, irregular patches, <10–20 cm across, to dyke networks with individual dykes 30–40 cm across and 3–4 m long (Fig. 4a). For clarity, we refer to these morphological end-members as patches and dykes, respectively, but

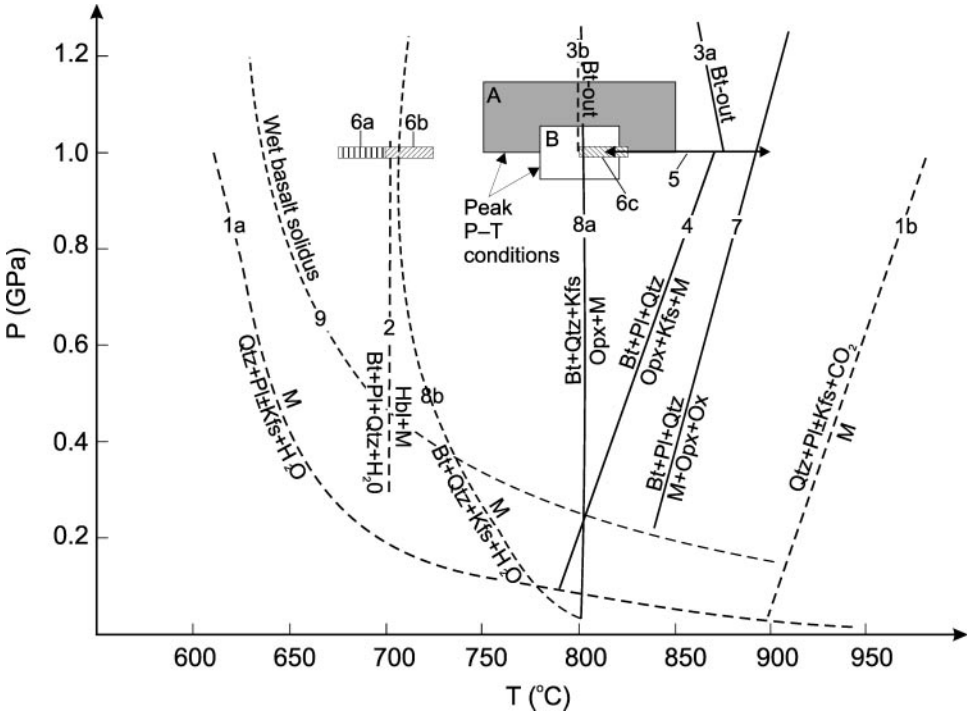

Fig. 3. *P–T* diagram summarizing some relevant melting reactions and results from experimental melting studies. For clarity, divariant reactions are illustrated using a single line. Continuous lines denote fluid-absent melting reactions, dashed lines denote fluid-present reactions. (1a) and (1b) illustrate the reaction Qtz + Pl ± Kfs + Fl = M in the presence of a pervasive H_2O-rich ($aH_2O = 1$) and CO_2-rich ($aH_2O = 0{\cdot}1$) fluid, respectively (Stevens & Clemens, 1993). (2) Water-saturated melting of tonalite Bt + Pl + Qtz + Fl (water-rich) = Hbl + M (Büsch *et al.*, 1974). (3) Partial melting of a biotite–plagioclase–quartz gneiss (Gardien *et al.*, 2000). (3a) Biotite-out with no H_2O added to the system. At pressures between 1 and 2 GPa and no H_2O added, <4 vol. % melt was produced at $T = 900°C$. (3b) Biotite-out with >2 wt % H_2O added. At pressures between 1 and 2 GPa and 4 wt % H_2O added, between 50 and 60 vol. % melt was produced at T as low as 800°C. (4) Fluid-absent melting Bt + Pl + Qtz = Opx + Kfs + M (Stevens & Clemens, 1993). (5) Fluid-absent biotite dehydration melting of a tonalite at 1 GPa (Rutter & Wyllie, 1988). Between 825 and 900°C (indicated by double-pointed arrow) the biotite melting reaction produced 20% melt. (6) Partial melting of dacite at 1 GPa (Conrad *et al.*, 1988). Boxes with vertical (6a), NE–SW diagonal (6b), and NW–SE diagonal (6c) lines represent the solidus at 1 GPa with $aH_2O = 0{\cdot}75$, 0·5, and 0·25, respectively. (7) Beginning of biotite dehydration melting in a biotite gneiss according to the reaction Bt + Pl + Qtz = M + Opx + Ox (Patiño Douce & Beard, 1995). (8a) Bt + Qtz + Kfs = Opx + M (reaction [V] of Peterson & Newton (1989)), and (8b) Bt + Qtz + Kfs + Fl (water-rich) = M (reaction [O] of Peterson & Newton (1989)). (9) Wet basalt solidus (Green, 1982). Boxes A (shaded) and B (white) indicate range of *P–T* conditions in the Muskoka domain determined by Timmermann *et al.* (2002) and S. Gagné & J. Hawken (unpublished data, 2002), respectively. Mineral abbreviations are after Kretz (1983); M, melt; Fl, fluid; Ox, oxides.

emphasize that the field, petrographic, and geochemical data strongly suggest that they are part of a continuum. Most of the patches contain coarse-grained granitic to pegmatitic-textured, strongly recrystallized leucosome, containing subhedral to euhedral, poikiloblastic hornblende up to 5 cm long (Fig. 4b and c). The inclusions are dominantly plagioclase, with minor quartz and biotite. The mineralogy of the patches varies from hornblende-dominated, with seam-like networks of granitic material, to leucosome-dominated, with little or no hornblende. The dykes are pegmatitic and typically zoned, with quartz-rich cores surrounded by K-feldspar-rich pegmatite (Fig. 4e), resembling typical pegmatite zonation and suggesting crystallization from relatively water-rich melts (e.g. Jahns & Burnham, 1969; Symmes & Ferry, 1995). Large hornblende crystals, morphologically resembling those in the patches, are common along the dyke margins (Fig. 4d) or form local accumulations within the dykes. Commonly, patches and dykes are connected by thin seams of granitic material oriented subparallel to the foliation in the dioritic mesosome. Immediately adjacent to the patches, and locally to the dykes, the host rock is enriched in subhedral, medium-grained (*c.* 0·5 cm) hornblende (Fig. 4c). These zones are interpreted as melanosome and referred to as patch melanosome below. Despite clear petrographic and geochemical differences, discussed below, the patch melanosomes are difficult to distinguish from the dioritic mesosome in the field. The distribution of melanosome is, therefore, unclear; in particular, some of the dykes appear to be locally intrusive and may lack associated melanosomes. Leucosome abundances are difficult to estimate in the patch migmatites because of their irregular distribution, but appear to be lower than in the stromatic migmatites.

In outcrops containing both stromatic and patch migmatites (e.g. Wren Lake outcrop), the foliation in the

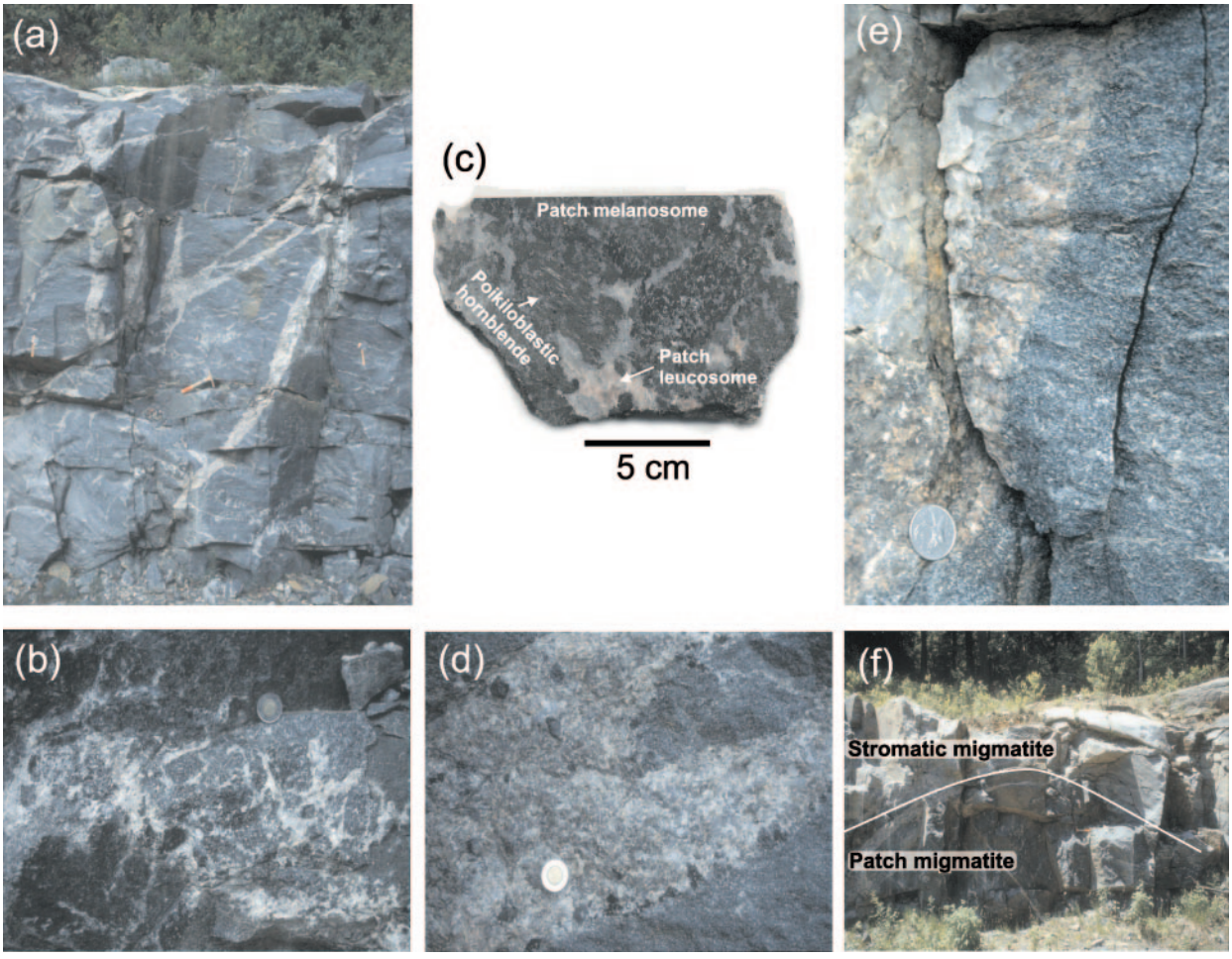

Fig. 4. (a) Network of dykes and patches in a patch migmatite; hammer for scale *c.* 30 cm long. (b) Hornblende-rich patch comprising subequal amounts of granitic leucosome and coarse hornblende; coin for scale *c.* 2·8 cm across. (c) Close-up of hornblende-rich patch showing coarse, subhedral, poikiloblastic hornblende and leucosome. (d) Close-up of pegmatite dyke with hornblende porphyroblasts, similar to those depicted in (b) and (c), concentrated along the margins; coin for scale *c.* 2·8 cm across. (e) Quartz-rich centre of zoned pegmatite dyke; coin for scale *c.* 2·4 cm across. (f) Foliation in the stromatic migmatites wrapping around a body of patch migmatite, forming a pinch-and-swell structure; field of view is *c.* 5 m across.

former can be seen wrapping around the latter, forming a pinch-and-swell structure (Fig. 4f). This observation suggests significant rheological contrast between the two types of migmatite. Unlike in the stromatic migmatites described below, there is no evidence that the location of the patch leucosomes is structurally controlled. We ascribe this difference to the higher strength of the dioritic host rocks relative to the surrounding granodioritic orthogneisses, which may have shielded the patch migmatites from the effects of deformation (see also Sawyer, 1999). None of the patches or dykes were observed to cut the patch–stromatic migmatite contact, thus the relative age of stromatic and patch migmatites is not known.

Stromatic migmatite

The stromatic migmatites are characterized by a layered structure made up of 0·5–5 cm thick layers of medium- to coarse-grained, strongly recrystallized granitic leucosome, typically a few metres long. The granodioritic host rock is commonly banded with centimetre-scale layers of dark grey diorite (Fig. 5a). The leucosomes are generally rimmed by thin, discontinuous melanosomes, referred to as concordant melanosome below. Leucosomes in the stromatic migmatites at Parkersville and Wren Lake range from concordant through slightly to strongly discordant to the host-rock foliation. Only concordant to slightly discordant leucosomes were sampled for geochemistry, and, for convenience, these leucosomes are referred to here as concordant leucosomes. The concordant leucosomes constitute 20–30 vol. %, and rarely up to 40–50 vol. %, of the stromatic migmatites, measured on a series of vertical cross-sections through the outcrops. The amount of leucosome varies strongly within an outcrop. At the Parkersville outcrop, for

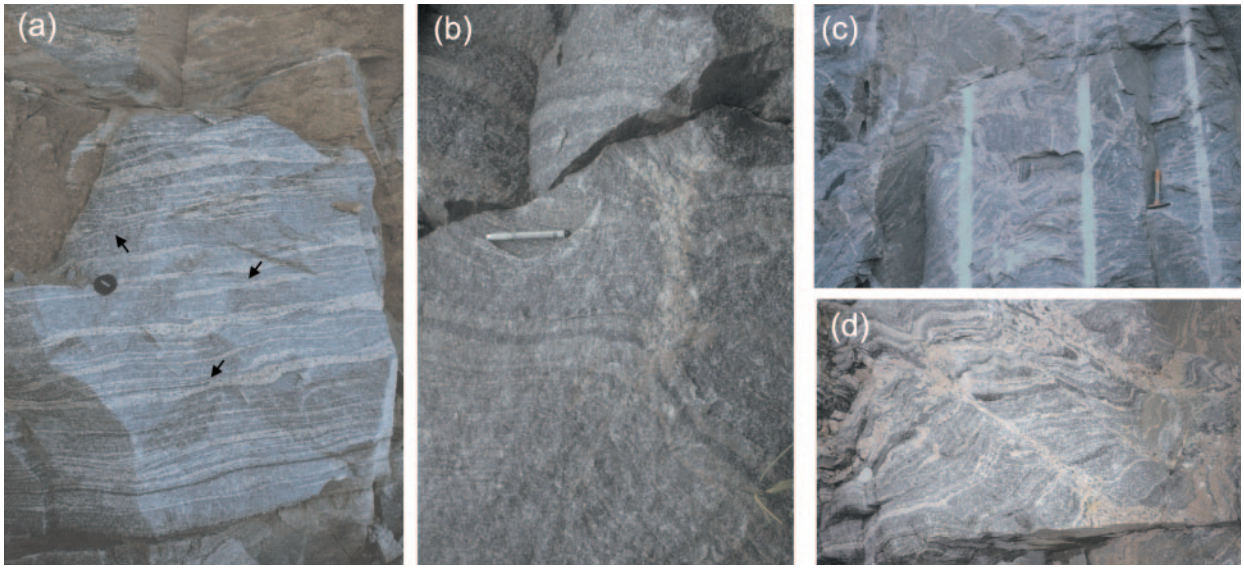

Fig. 5. (a) Concordant leucosome in stromatic migmatite. Arrows indicate locations where a discordant relationship is observed between different generations of leucosome; lens cap for scale *c.* 5 cm across. (b) Small leucosome patch in boudin neck; pen for scale *c.* 13 cm long. (c) Part of outcrop with a very large proportion of leucosome, containing small, rotated blocks of 'normal' stromatic migmatite; hammer for scale *c.* 30 cm long. (d) Discordant leucosome in small shear bands; field of view is *c.* 1 m across (vertical view).

example, leucosome abundances range from <5 to *c.* 50 vol. % over a distance of a few tens of metres. We could not, however, identify any gradual variation between leucosome-poor and -rich parts of the outcrop. Locally, where leucosome proportions reach 40–50 vol. %, the stromatic migmatites contain rotated 'blocks' of migmatitic gneiss 'floating' in leucosome (Fig. 5c). The concordant leucosomes are variably folded and, in places, younger leucosomes can be seen cutting older, deformed leucosomes (Fig. 5a); the observed 20–50 vol. % leucosome is therefore cumulative, and is unlikely to represent the amount of melt present at any one time, nor does it represent the fraction of melt (F) generated by melting of the mesosome. Locally, the melts appear to have migrated along foliation planes and accumulated within shear bands or in boudin necks (Fig. 5b). These observations suggest that melting and/or melt movement in the rocks was coeval with deformation (e.g. Collins & Sawyer, 1996; Timmermann *et al.*, 2002).

The very high leucosome proportions observed in the stromatic migmatites (e.g. in the Parkersville outcrop) are inconsistent with *in situ* partial melting, both because granodioritic gneisses are unlikely to yield such high melt proportions and because complementary residual rocks are missing. Although the concordant melanosomes may represent residues after partial melting, the small volume of melanosome (typically only 1–2 mm thick) cannot account for the volume of leucosome in the rocks. A rigorous mass balance calculation is precluded by difficulties in estimating the composition of the concordant melanosome and the interpretation (below) that most of the leucosomes do not represent melt compositions.

The contrast in geometry between the patch and stromatic migmatites could result from differences in the timing of leucosome formation (i.e. patch migmatites formed post-kinematically) and/or from local differences in strain during deformation.Geochronological data from the stromatic migmatites indicate that the concordant leucosomes crystallized at *c.* 1065 Ma (Timmermann *et al.*, 1997; Slagstad *et al.*, 2004*b*), and that high-grade metamorphism and deformation persisted until *c.* 1050 Ma; thus it is possible that the patch migmatites formed later in the metamorphic history of the Muskoka domain and therefore experienced less deformation.The available field and geochronological data neither support nor reject this hypothesis. In contrast, there is good field evidence to suggest a significant rheological contrast between the two types of migmatite and we believe that this contrast may have been the main factor controlling the geometry of the leucosomes. Although the exact mechanism by which stromatic structures develop is obscure, work by Robin (1979) and Brown *et al.* (1995) suggests that they can develop in response to applied differential stress acting on a strongly anisotropic protolith, such as the banded, granodioritic host rock to the stromatic migmatites. In contrast, the dioritic host rock to the patch migmatites was stronger and more homogeneous, possibly resulting in a stress field that was closer to isotropic, favouring the observed patch geometry. At present, this is our preferred hypothesis for the geometrical differences between the patch and stromatic migmatites.

PETROGRAPHY AND GEOCHEMISTRY

Analytical procedures

Major and trace elements were determined on fused glass beads and pressed powder pellets, respectively, using standard X-ray fluorescence (XRF) techniques at St. Mary's University, Halifax, Nova Scotia. Rare earth elements (REE), Hf, and Th were determined by inductively coupled plasma-mass spectrometry (ICP-MS) using a Na_2O_2 sintering technique at Memorial University, St. John's, Newfoundland. Dostal *et al.* (1986) and Longerich *et al.* (1990) discussed the analytical procedures, accuracy, and precision of the XRF and ICP-MS analyses, respectively. The geochemical data are presented in Tables 1 and 2; modes of representative samples are presented in Table 3. Mineral abbreviations used in the text and figures are from Kretz (1983).

Patch migmatite

The dioritic mesosome is fine grained, with a granoblastic to weakly foliated texture, dominantly comprising hornblende and plagioclase with minor biotite and quartz. Biotite laths, typically 1–3 mm long, define a weak foliation. Apatite and zircon are the main accessory minerals; allanite was not observed.

The patches are characterized by a mix of medium- to coarse-grained granitic leucosome (patch leucosome) with large (1–5 cm long), randomly oriented, euhedral to subhedral, poikiloblastic or skeletal hornblende (Figs. 4b, c and 6d). Plagioclase inclusions are abundant and typically constitute 30–40 vol. % of the poikiloblastic hornblendes, along with minor quartz and biotite inclusions. The plagioclase inclusions are typically irregular and many are oriented roughly along the cleavage of the hornblende. We interpret this texture to indicate that the hornblendes crystallized in the presence of melt, and their random orientation suggests minimal post-crystallization strain.

The patches grade into melanosome comprising medium-grained ($\sim$0·5 cm) hornblende (60–70 vol. %), plagioclase (30–40 vol. %), and minor biotite. This type of melanosome is referred to as patch melanosome to distinguish it from the concordant melanosome in the stromatic migmatites. Coarse hornblende in the patch melanosome typically contains rounded inclusions of plagioclase, biotite, and quartz. Biotite typically forms dark red to nearly opaque, corroded grains, in contrast to the fine biotite laths in the dioritic mesosome.

The dykes are pegmatitic but otherwise petrographically similar to the patch leucosomes. Along their margins, the dykes contain significant amounts of hornblende; some of this hornblende is texturally similar to the large, poikiloblastic hornblende in the patches, and some is similar to hornblende in the patch melanosome.

The dioritic mesosome and patch melanosome have overlapping major element compositions, but on average, the melanosome is lower in SiO_2, Al_2O_3, and Na_2O, and higher in TiO_2, Fe_2O_3, MgO, and CaO (Fig. 7). The K_2O content is similar in the mesosome and melanosome. The patch leucosomes and pegmatite dykes are enriched in SiO_2 and K_2O relative to the mesosome and melanosome, but depleted in the other major elements. Apart from patch leucosome sample M30072-3-L2, the leucosomes and dykes have K_2O >5·9 wt %, unusually high for granitic melts. This is illustrated in the normative Q–Ab–Or diagram (Fig. 7h), where the patch leucosomes and dykes are displaced towards the Or apex relative to cotectic melts. In contrast, sample M30072-3-L2 plots closer to the eutectic composition for melts formed under water-undersaturated conditions corresponding to $a H_2O$ $\sim$0·5 at *c.* 1 GPa (Johannes & Holtz, 1990). Sample M30072-3-L2 is enriched in Al_2O_3, CaO, and Na_2O, and depleted in K_2O relative to the other patch leucosomes, indicating a higher plagioclase/K-feldspar ratio in this sample than in the other leucosomes.

Complete separation of melanosome from leucosome prior to analysis was generally achieved for the leucosome samples, whereas the sampled melanosome probably contains several percent leucosome. The effect of 'contamination' by 5–10 wt % leucosome is relatively minor for most major elements (<10–15%), but not for K_2O, which increases by several tens of percent. The measured K_2O content of the patch melanosome is, therefore, likely to be too high. The patch leucosomes are low in REE compared with the melanosomes (see below), thus 'contamination' by leucosome does not affect REE contents of the melanosome significantly.

The patch leucosomes and dykes are enriched in trace elements associated with feldspar (Ba, Rb, Sr) but depleted in other trace elements relative to the dioritic mesosome and patch melanosome. The patch leucosomes and dykes show a negative correlation between K_2O and both Na_2O and CaO, but a positive correlation between K_2O and Rb/Sr (Fig. 8c), indicating that crystallization of feldspar was a major factor in the compositional variation of the leucosomes. The REE correlate with P_2O_5, Zr, Hf, Y, and Nb indicating that accessory apatite and zircon exerted a significant control on the behaviour of the REE. The $(La/Yb)_N$ ratios vary little within the patch migmatites, ranging from about five in the dioritic mesosome and patch melanosome to *c.* 10 in the patch leucosomes; the dykes have significantly higher $(La/Yb)_N$ ratios ranging from nine to 90. The Eu anomalies $[(Eu/Eu^*)_N]$ of the patch leucosomes are inversely correlated with total REE (Fig. 8), increasing from 0·75 in the most REE-rich sample to 1·79 in the sample with

Table 1: Geochemistry of the stromatic migmatites

	Granodioritic mesosome								
	Parkersville				Wren Lake				
Sample:	M03083B-M1	M03083B-M2	M03083B-M3	M03083B-M4	M2707-16B-M2	M2707-16B-M4	M2707-16B-M5	M2707-16B-M7	M2707-16B-M8
wt %									
SiO_2	65·25	65·03	66·62	66·11	67·99	67·57	65·84	65·25	66·52
TiO_2	0·60	0·61	0·65	0·61	0·55	0·59	0·71	0·71	0·70
Al_2O_3	15·45	15·42	15·67	15·64	15·12	15·33	15·01	15·54	15·14
Fe_2O_3	4·49	4·54	4·72	4·40	4·01	4·15	4·26	5·01	4·88
MnO	0·08	0·07	0·08	0·07	0·06	0·05	0·06	0·07	0·08
MgO	1·43	1·42	1·51	1·41	1·31	1·48	1·50	1·84	1·88
CaO	3·42	3·40	3·59	3·42	2·87	3·01	3·00	3·45	3·54
Na_2O	3·92	4·14	4·10	4·05	3·71	3·89	4·01	4·06	4·06
K_2O	3·87	3·63	3·90	3·65	3·96	3·84	4·25	2·97	2·70
P_2O_5	0·18	0·18	0·20	0·18	0·16	0·17	0·18	0·20	0·19
LOI	0·28	0·44	0·50	0·40	0·38	0·10	0·57	0·40	0·46
Total	98·97	98·89	101·54	99·94	100·12	100·18	99·39	99·51	100·15
ppm									
Ba	957	924	890	945	955	962	1231	598	721
Rb	104	102	100	102	98	99	99	88	79
Sr	387	382	418	402	330	332	389	317	338
Y	35	35	37	35	47	42	43	48	60
Zr	236	237	262	225	264	297	373	316	230
Nb	13	11	8	11	11	13	17	13	16
Th	11·11	13·33	11·11	11·09	8·84	8·62	4·62	8·39	3·99
Ga	19	17	18	17	16	18	15	21	19
Zn	68	70	72	69	60	67	66	78	80
Ni	9	8	7	10	8	<3	5	8	5
V	85	82	90	83	74	82	88	92	90
Cr	<4	<4	<4	<4	6	5	7	12	16
Hf	7·40	6·28	7·56	5·80	6·32	7·76	9·32	8·84	6·30
Co	47	49	47	45	69	54	78	65	64
U	2	2	2	2	2	2	2	2	2
La	46·55	53·03	48·32	44·40	64·94	61·27	49·41	67·32	48·20
Ce	95·44	107·65	100·63	91·53	127·51	123·14	110·54	142·31	110·88
Pr	11·10	12·33	11·76	10·76	15·08	14·46	14·27	17·43	15·02
Nd	42·11	46·44	45·69	40·63	56·66	54·16	56·97	68·09	62·65
Sm	7·95	8·61	8·74	7·30	10·76	10·09	10·65	12·51	13·56
Eu	1·40	1·49	1·53	1·30	1·40	1·35	1·41	1·50	1·43
Gd	6·29	6·76	7·07	6·32	8·57	7·86	8·18	9·68	11·28
Tb	0·99	1·08	1·14	0·98	1·31	1·19	1·35	1·57	1·91
Dy	6·05	6·47	6·92	6·04	8·14	7·26	8·18	9·56	11·73
Ho	1·27	1·35	1·46	1·20	1·53	1·36	1·61	1·86	2·31
Er	3·79	4·01	4·33	3·55	4·57	4·00	4·76	5·42	6·80
Tm	0·57	0·59	0·65	0·54	0·68	0·59	0·72	0·80	1·01
Yb	3·84	4·02	4·38	3·63	4·46	3·84	4·80	5·16	6·49
Lu	0·58	0·60	0·66	0·52	0·65	0·57	0·67	0·72	0·89

Table 1: continued

	Concordant leucosomes									
	Parkersville					Wren Lake				
Sample:	M03083B-L1	M03083B-L3	M03083B-L4	2M02061-9A	2M02061-9B	M2707-16-L1	M2707-16B-L1	M2707-16B-L3	M2707-16B-L5	2M0506-15
wt %										
SiO_2	72·60	71·92	70·19	72·95	69·85	73·57	72·85	70·50	70·54	70·43
TiO_2	0·15	0·15	0·22	0·15	0·31	0·17	0·14	0·29	0·25	0·21
Al_2O_3	14·12	13·81	14·14	14·03	15·76	14·44	14·13	14·75	14·47	14·29
Fe_2O_3	1·14	1·22	1·61	1·31	1·94	1·33	0·91	2·00	1·62	1·36
MnO	0·01	0·01	0·02	0·02	0·04	0·01	0·01	0·03	0·02	0·02
MgO	0·20	0·19	0·38	0·22	0·54	0·23	0·21	0·59	0·37	0·51
CaO	1·58	1·53	2·02	1·81	2·09	1·08	1·27	1·89	1·72	1·43
Na_2O	2·89	3·02	3·41	3·24	3·23	2·52	2·64	2·99	3·20	2·59
K_2O	6·57	6·98	6·44	5·83	6·53	7·57	6·76	6·66	6·81	6·95
P_2O_5	0·03	0·03	0·05	0·03	0·08	0·04	0·04	0·07	0·07	0·05
LOI	0·37	0·47	0·47	0·19	0·30	0·38	0·27	0·21	0·10	0·89
Total	99·67	99·33	98·95	99·59	100·36	101·34	99·22	99·98	99·16	97·84
ppm										
Ba	1631	1763	1741	2069	2741	1609	1565	1777	1777	1771
Rb	153	158	142	136	152	157	139	124	128	138
Sr	448	459	454	479	531	383	408	442	450	460
Y	13	14	19	12	20	17	19	28	21	12
Zr	133	129	146	129	263	159	153	212	216	131
Nb	2	2	9	1	4	2	2	11	10	3
Th	13·12	12·24	11·48	10·21	9·91	11·58	13·84	6·66	10·55	6·09
Ga	14	15	15	15	18	13	13	14	16	14
Zn	19	21	29	20	31	21	14	30	26	24
Ni	11	18	7	14	<3	5	5	<3	<3	<3
V	29	28	37	32	45	29	26	43	41	36
Cr	<4	<4	<4	<4	<4	<4	<4	<4	<4	<4
Hf	3·08	3·15	4·47	2·99	5·31	3·68	4·35	6·02	6·03	3·00
Co	77	83	72	92	46	75	77	64	75	58
U	3	2	2	4	4	3	2	2	2	3
La	24·10	21·89	31·05	22·03	28·51	40·00	42·97	31·08	29·45	28·64
Ce	46·57	42·92	60·60	42·49	53·52	83·64	90·19	66·30	58·71	48·16
Pr	4·90	4·62	6·61	4·63	5·96	9·67	10·39	8·29	6·82	4·89
Nd	16·07	15·22	23·59	15·84	21·98	34·34	35·96	32·42	24·90	16·21
Sm	2·44	2·46	3·82	2·25	3·59	4·67	5·20	6·24	4·29	2·77
Eu	0·80	0·80	1·08	0·83	1·37	1·19	1·30	1·43	1·23	1·02
Gd	1·75	1·88	2·79	1·71	3·06	3·14	3·40	5·16	3·32	1·93
Tb	0·25	0·28	0·44	0·24	0·44	0·42	0·46	0·77	0·49	0·29
Dy	1·49	1·66	2·63	1·44	2·73	2·37	2·62	4·73	2·93	1·61
Ho	0·26	0·29	0·55	0·28	0·54	0·45	0·49	0·91	0·55	0·27
Er	0·83	0·94	1·70	0·85	1·63	1·26	1·44	2·66	1·62	0·72
Tm	0·12	0·13	0·26	0·13	0·25	0·18	0·21	0·40	0·24	0·10
Yb	0·80	0·91	1·81	0·87	1·73	1·21	1·42	2·64	1·62	0·65
Lu	0·13	0·15	0·27	0·13	0·27	0·18	0·20	0·38	0·25	0·11

Table 2: Geochemistry of the patch migmatites

	Dioritic mesosome										
	Bonnie Lake								Wren Lake		
Sample:	M2707-10-M1	M2707-10-M2	2M0506-10	2M0506-11	2M1506-2 M	M2707-5-M2	2M0506-12D	2M0506-14B	M30072-1-M	M30072-3-M1	M30072-3-M2
wt %											
SiO_2	48·24	47·98	54·24	51·14	52·08	49·33	50·40	50·44	51·72	52·30	47·65
TiO_2	1·60	1·69	0·93	1·29	1·16	1·30	1·26	1·39	1·24	1·01	1·65
Al_2O_3	17·47	17·69	16·39	18·38	16·61	16·39	17·35	16·60	16·60	17·26	17·32
Fe_2O_3	12·60	12·88	8·50	10·00	10·37	11·30	10·83	11·31	11·27	9·61	12·27
MnO	0·20	0·20	0·14	0·15	0·18	0·20	0·21	0·23	0·25	0·17	0·18
MgO	4·52	4·50	4·88	3·83	4·54	5·65	4·86	4·74	4·75	5·24	6·44
CaO	8·05	8·11	7·80	7·56	8·17	8·56	8·37	8·06	7·42	8·47	7·82
Na_2O	3·95	4·01	3·92	4·17	3·93	3·91	4·23	4·11	3·57	3·79	3·25
K_2O	2·02	1·94	2·14	2·40	1·94	1·83	1·80	1·68	1·83	1·56	2·84
P_2O_5	0·49	0·51	0·28	0·38	0·34	0·38	0·39	0·43	0·19	0·20	0·32
LOI	0·40	0·54	0·79	0·50	0·50	0·57	0·70	0·20	0·54	0·38	0·52
Total	99·54	100·05	106·86	108·30	108·65	99·42	109·44	109·17	99·38	99·98	100·26
ppm											
Ba	854	771	613	925	710	213	458	301	300	200	508
Rb	54	123	46	72	32	45	27	21	55	31	90
Sr	537	567	603	854	562	455	553	535	488	531	456
Y	37	37	38	33	43	43	75	79	51	30	40
Zr	324	383	200	530	275	245	321	239	206	183	174
Nb	12	12	9	7	11	17	16	23	20	12	18
Th	2·91	2·81	3·22	n.a.	n.a.	4·53	3·78	2·50	1·91	2·46	2·41
Ga	23	24	21	23	22	26	26	24	26	22	24
Zn	138	138	118	115	133	162	161	158	171	112	150
Ni	9	7	34	13	7	41	22	23	4	13	37
V	250	248	151	191	191	223	190	214	236	186	272
Cr	7	<4	115	30	35	114	73	66	6	30	37
Hf	8·53	8·72	4·66	n.a.	n.a.	6·76	9·12	7·03	5·73	4·63	4·54
Co	36	54	57	47	61	36	50	55	50	31	39
U	<1	2	<1	<1	1	1	1	1	<1	1	1
La	41·32	38·71	35·26	n.a.	n.a.	58·90	65·81	57·89	27·14	28·07	33·58
Ce	95·09	89·35	80·66	n.a.	n.a.	144·71	173·00	156·49	84·94	68·31	86·09
Pr	12·72	11·99	10·76	n.a.	n.a.	19·23	24·40	22·23	13·29	9·05	12·31
Nd	54·72	50·50	44·50	n.a.	n.a.	77·52	101·77	93·19	56·79	36·84	53·19
Sm	10·90	9·99	9·00	n.a.	n.a.	14·45	20·78	18·82	11·64	7·43	11·18
Eu	2·80	2·51	1·71	n.a.	n.a.	2·41	2·95	2·55	2·25	1·74	1·98
Gd	10·48	9·57	8·15	n.a.	n.a.	11·40	18·17	17·20	10·56	6·73	10·03
Tb	1·59	1·46	1·27	n.a.	n.a.	1·68	2·76	2·63	1·69	1·03	1·48
Dy	9·67	8·94	7·91	n.a.	n.a.	10·17	16·97	16·23	11·07	6·40	9·39
Ho	1·91	1·76	1·45	n.a.	n.a.	1·96	3·24	3·17	2·37	1·31	1·95
Er	5·46	5·08	4·32	n.a.	n.a.	5·78	9·50	9·44	7·32	3·88	5·89
Tm	0·78	0·74	0·65	n.a.	n.a.	0·88	1·40	1·40	1·15	0·60	0·89
Yb	5·11	4·76	4·33	n.a.	n.a.	6·22	9·07	9·20	7·94	4·20	6·06
Lu	0·72	0·69	0·64	n.a.	n.a.	0·95	1·33	1·29	1·14	0·65	0·92

Table 2: continued

	Patch leucosome					Pegmatite dykes					Patch melanosome
	Wren Lake			Bonnie Lake		Wren Lake					Wren Lake
Sample:	M2707-5-L1	M2707-5-L2	M2707-5B-L	M30072-3-L1	M30072-3-L2	2M0506-17	2M0506-6	2M0506-7	2M0506-8	2M0506-12A	M2707-5B-M
wt %											
SiO_2	73·77	70·26	68·15	70·99	64·34	75·21	72·74	70·23	74·71	71·11	46·43
TiO_2	0·16	0·22	0·38	0·22	0·35	0·12	0·03	0·17	0·09	0·12	1·56
Al_2O_3	13·16	14·04	13·60	14·45	16·68	14·42	14·62	14·92	13·87	15·00	14·80
Fe_2O_3	1·63	1·99	3·28	1·83	3·39	0·82	0·26	1·53	0·94	1·55	14·98
MnO	0·02	0·03	0·05	0·02	0·05	0·01	0·00	0·02	0·01	0·01	0·25
MgO	0·66	0·87	1·32	0·97	1·76	0·24	0·16	0·54	0·32	0·15	6·75
CaO	1·56	1·64	2·16	2·37	5·24	1·39	0·31	1·08	1·08	0·55	8·96
Na_2O	2·09	1·96	2·06	2·42	3·83	3·02	2·09	2·34	2·34	2·09	3·22
K_2O	6·99	8·14	6·93	6·19	3·09	5·92	9·08	8·15	6·90	9·13	1·91
P_2O_5	0·05	0·07	0·09	0·04	0·16	0·02	0·02	0·03	0·02	0·02	0·43
LOI	0·72	1·18	0·88	1·15	0·72	0·30	0·55	0·91	0·21	0·30	0·87
Total	100·81	100·40	98·90	100·66	99·61	101·17	99·31	99·01	100·29	99·72	100·16
ppm											
Ba	2087	2396	2399	2765	1365	1653	3171	3002	2542	3252	225
Rb	249	281	225	136	64	150	235	208	179	226	42
Sr	609	657	612	649	657	493	647	670	639	712	370
Y	12	15	24	12	22	<5	<5	16	11	<5	54
Zr	154	128	140	83	146	54	54	172	50	295	290
Nb	4	4	8	4	10	<1	<1	2	1	<1	23
Th	1·54	49·45	3·04	6·57	1·44	3·96	0·86	4·38	3·81	1·37	3·84
Ga	10	9	14	11	17	16	11	16	13	13	31
Zn	24	31	44	22	50	16	<5	28	12	14	201
Ni	23	16	24	<3	5	<3	11	16	5	114	46
V	33	42	66	44	71	27	16	35	26	35	259
Cr	8	9	26	<4	<4	<4	<4	<4	<4	26	151
Hf	3·11	2·17	2·82	1·30	3·22	0·80	0·47	3·15	0·32	5·91	8·44
Co	121	124	66	91	79	85	101	66	65	76	57
U	1	4	<1	2	<1	3	2	2	2	2	<1
La	15·48	20·82	24·57	12·77	18·74	20·27	6·84	14·19	15·63	7·36	62·25
Ce	26·95	36·06	52·54	19·67	37·65	31·24	6·78	25·47	23·68	7·54	172·39
Pr	3·08	4·03	6·69	2·15	4·73	2·98	0·53	3·16	2·68	0·61	23·88
Nd	11·70	14·68	26·81	8·08	19·13	9·14	1·46	12·87	9·62	1·70	99·37
Sm	2·05	2·49	5·17	1·38	3·77	1·08	0·16	2·94	1·80	0·25	19·32
Eu	0·87	0·91	1·20	0·76	1·04	1·05	0·92	1·28	1·06	1·04	2·88
Gd	1·60	1·97	4·37	1·15	3·30	0·63	0·12	2·64	1·43	0·19	15·67
Tb	0·24	0·29	0·66	0·17	0·50	0·07	0·02	0·40	0·24	0·03	2·38
Dy	1·47	1·79	4·17	1·09	3·11	0·37	0·08	2·46	1·47	0·18	14·24
Ho	0·29	0·35	0·81	0·23	0·65	0·06	0·02	0·43	0·28	0·04	2·75
Er	0·85	1·06	2·38	0·68	1·94	0·17	0·05	1·25	0·83	0·13	8·08
Tm	0·13	0·16	0·36	0·11	0·30	0·02	0·01	0·18	0·12	0·03	1·21
Yb	0·95	1·14	2·48	0·78	2·13	0·17	0·06	1·19	0·76	0·22	8·39
Lu	0·15	0·18	0·37	0·12	0·33	0·03	0·01	0·19	0·12	0·05	1·27

Table 3: Modes of representative migmatite samples

Sample:	Granodioritic mesosome M03083B-M	Concordant leucosome M2707-16	Concordant melanosome M2707-16B-5	Dioritic mesosome M2707-10	Patch leucosome M2707-5-L2	Patch melanosome M2707-5B-M
Quartz	15·0	31·3	5·5	acc.	25·8	
Plagioclase	53·8	24·1	56·0	46·3	4·0	23·0
K-feldspar	11·0	37·8	1·0		62·0	
Hornblende	11·6	0·8	16·5	37·5	4·0	56·0
Biotite	6·8	4·0	20·0	8·0	1·0	17·0
Opaques	1·6	1·8	acc	8·3	n.d.	3·8
Apatite	acc.	n.d.	acc	acc.	n.d.	acc.
Zircon	acc.	acc.	acc	acc.	n.d.	acc.
Allanite	acc.	n.d.	acc.	n.d.	n.d.	n.d.

Mode based on 400–600 counts per sample. acc., accessory phase (<0·25 vol. %); n.d., not detected.

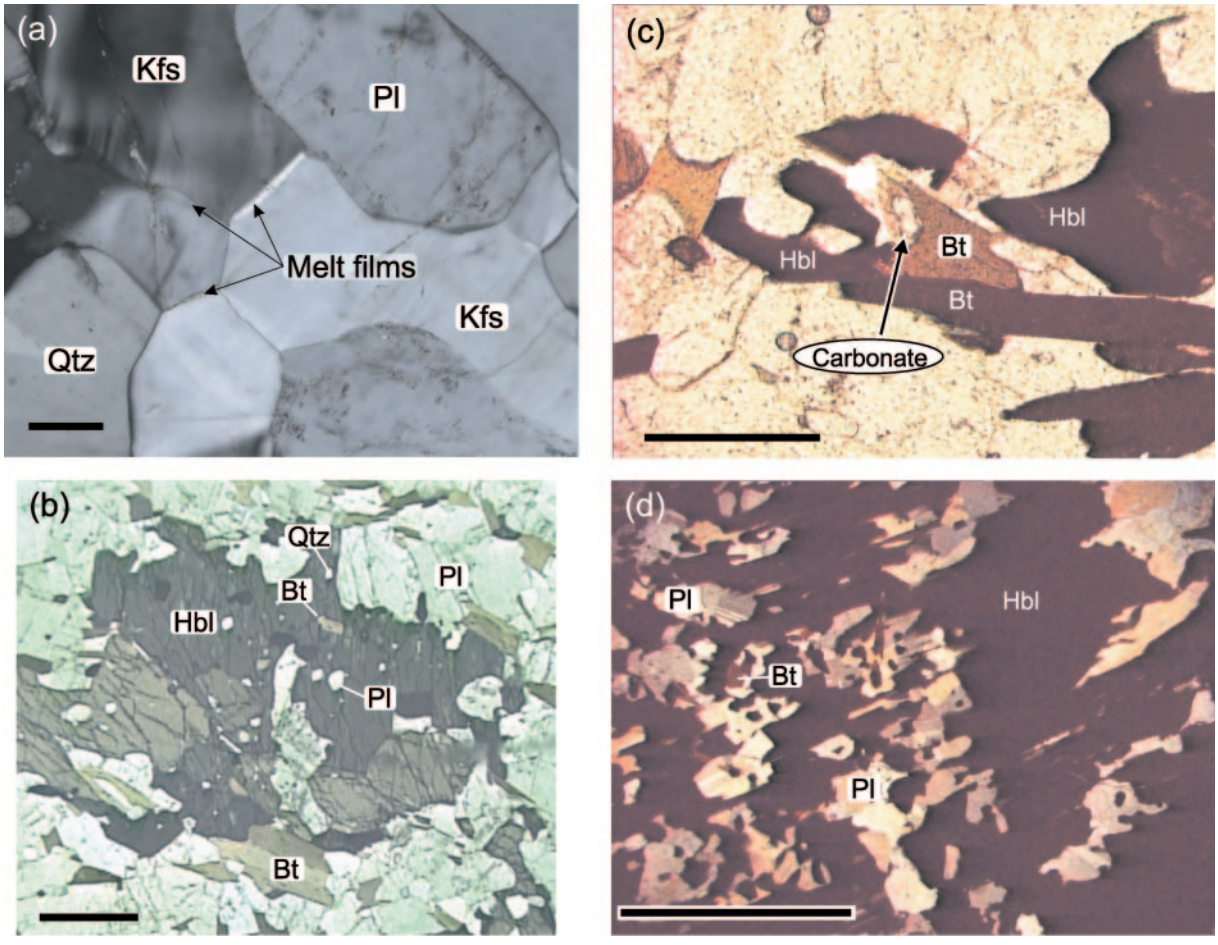

Fig. 6. (a) 'Melt' films along K-feldspar grain boundaries in granodioritic mesosome, from Parkersville outcrop. Similar 'melt' films have been observed in the dioritic mesosome. Scale bar represents 0·1 mm. (b) Coarse hornblende with rounded inclusions of plagioclase, biotite, and quartz from the concordant melanosome, from Parkersville outcrop. Coarse biotite on the right-hand side of the photograph is apparently in equilibrium with the hornblende. Scale bar represents 1 mm. (c) Small carbonate grain associated with biotite in granodioritic mesosome at Parkersville outcrop. Scale bar represents 0·5 mm. (d) Coarse, subhedral hornblende porphyroblast (dark) with abundant plagioclase inclusions in hornblende-rich patch, from Wren Lake outcrop. The hornblende is optically continuous. Scale bar represents 5 mm.

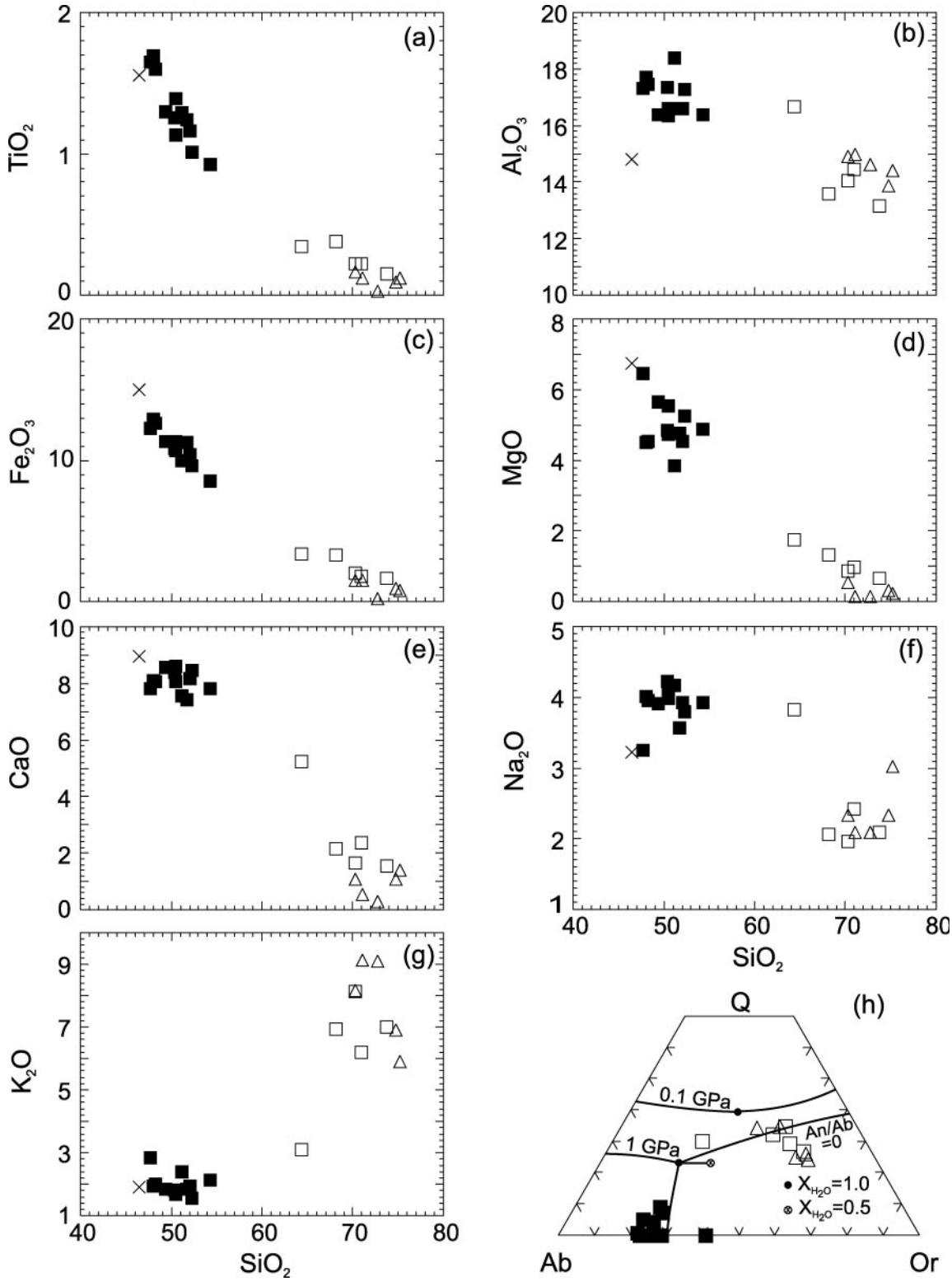

Fig. 7. Harker variation diagrams and normative Q–Ab–Or ternary diagram, showing the compositions of patch migmatites. ■, dioritic mesosome; □, patch leucosome; △, dykes; ×, patch melanosome.

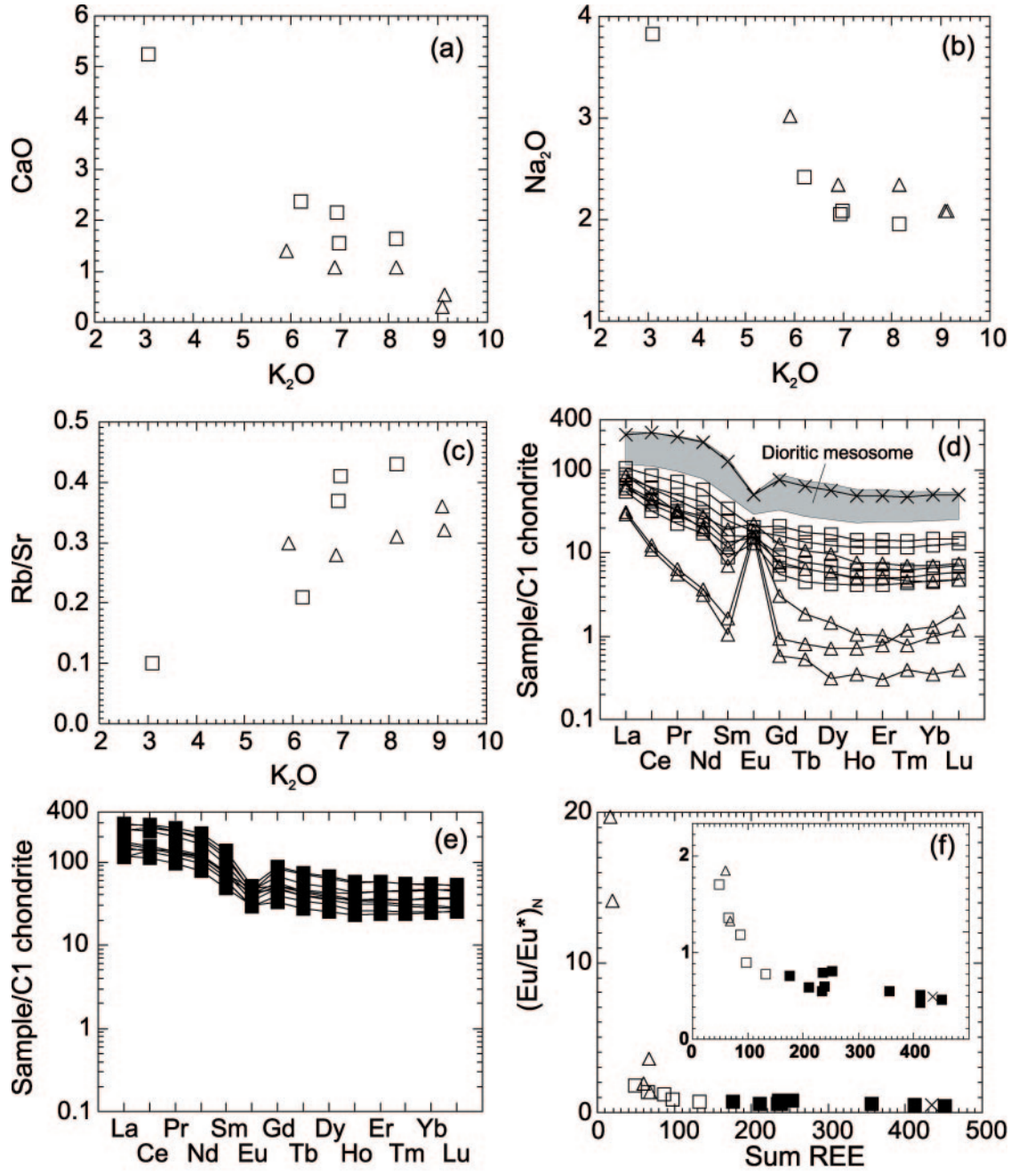

Fig. 8. Major and trace element bivariate diagrams for the patch leucosomes and dykes, and chondrite-normalized REE patterns for the patch migmatites comparing the different migmatite components. Normalized to values of Sun & McDonough (1989). Symbols as in Fig. 7.

lowest total REE. In the dykes, $(Eu/Eu^*)_N$ ratios increase from 1·37 to 19·67 with decreasing total REE content. Despite significant major element differences between patch leucosome sample M30072-3-L2 and the other patch leucosomes/dykes, the trace element contents are similar and fall along the same trends.

Stromatic migmatites

The concordant leucosomes and granodioritic mesosomes were sampled by serial cutting of large slabs. The concordant melanosomes were too thin to be sampled for geochemical analysis. Timmermann (1998) and Timmermann *et al.* (2002) described the petrography of

the stromatic migmatites in the Muskoka domain in detail, and the following description therefore focuses on features pertinent to their petrogenesis.

The granodioritic to quartz monzodioritic mesosome (for simplicity referred to as granodioritic) is fine to medium grained and moderately foliated. Minor, interstitial 'melt films' (see Sawyer, 2001) along some grain boundaries (Fig. 6a) and rare, small (<1 cm) quartz–feldspar patches, interpreted to represent former melt patches, suggest some melting in the mesosome. However, there is no petrographic or geochemical evidence that significant volumes of melt were extracted from the mesosome. The proportion of melt films in the granodioritic mesosome, estimated by point counting as <0·5‰, is volumetrically insignificant. Apatite, zircon, and allanite are common accessory phases.

The concordant leucosomes are medium to coarse grained and granitic, with *c.* 1–5 vol. % hornblende porphyroblasts and flakes of biotite. The hornblende in the leucosomes is texturally similar to that found in the associated concordant melanosomes, and probably represents residual hornblende that was mechanically incorporated into the melt.

The concordant melanosomes are generally <5–10 mm thick and comprise hornblende, plagioclase, and biotite with accessory apatite, zircon, allanite, and titanite. Much of the hornblende in the concordant melanosome is texturally similar to hornblende in the granodioritic mesosome; however, a significant portion is coarser grained with rounded inclusions of plagioclase, quartz, and biotite (Fig. 6b); that is, similar to the patch melanosomes. Similar coarse hornblende is absent from the granodioritic mesosome. Coarse plagioclase with inclusions of biotite and quartz is common in the concordant melanosomes. Biotite in the concordant melanosomes is compositionally similar to biotite in the granodioritic mesosome, but is coarser and forms clusters intergrown and apparently in equilibrium with hornblende (Fig. 6b). However, the *P–T* conditions experienced by these rocks (Timmermann *et al.*, 2002; S. Gagné & J. Hawken, unpublished data, 2002) suggest that biotite was unlikely to have been stable during peak metamorphism (Fig. 3); it seems more likely that the biotite in the concordant melanosomes grew during retrograde reaction with the melt as the melt crystallized (see Waters, 2001).

The granodioritic mesosome ranges from 65 to 68 wt % SiO_2. Samples from the two investigated outcrops at Parkersville and Wren Lake have similar major (Fig. 9) and trace element contents. The granodioritic mesosome from Wren Lake is slightly higher in total REE with more pronounced negative Eu anomalies [$(Eu/Eu^*)_N = 0{\cdot}40$–$0{\cdot}45$] than mesosome from Parkersville [$(Eu/Eu^*)_N = 0{\cdot}58$], but the REE patterns are similarly fractionated [$(La/Yb)_N = 5$–12] (Fig. 10).

The concordant leucosomes contain 70–73 wt % SiO_2; although clustered, most major elements decrease with increasing SiO_2 (Fig. 9) whereas K_2O and most trace elements show little systematic variation. As for the patch leucosomes, K_2O is negatively correlated with CaO and Na_2O, and positively correlated with Rb/Sr, suggesting crystallization of feldspar. In the normative Q–Ab–Or diagram (Fig. 9h) the concordant leucosomes plot close to the cotectic line separating the primary fields for quartz and K-feldspar, similar to the patch leucosomes. The REE patterns (Fig. 10b) are moderately fractionated, with $(La/Yb)_N$ increasing from eight to 24 with increasing SiO_2 (Fig. 10c). Total REE and Eu anomalies [$(Eu/Eu^*)_N = 0{\cdot}7$–$1{\cdot}3$] are negatively correlated (Fig. 10d), but neither are correlated with SiO_2.

Relative to the granodioritic mesosome, the concordant leucosomes are depleted in all major elements except SiO_2 and K_2O. Barium, Rb, and Sr are enriched in the leucosomes. Yttrium, Zr, Hf, and Nb are lower in the leucosomes, and Th is similar in leucosomes and granodioritic mesosomes. Total REE contents are lower, REE patterns more fractionated, and Eu anomalies are more positive in the leucosomes than in the mesosomes (Fig. 10a and b).

MIGMATITE PETROGENESIS

Evidence for fluid-present partial melting

Feldspars, quartz, hornblende, and biotite in variable proportions dominate the mineralogy of the mesosome, melanosome, and leucosome in both types of migmatite. Despite the relatively simple mineralogy, the textures described above provide some clues to the melting reactions in these rocks. In both the patch and concordant melanosome, coarse-grained hornblende with numerous rounded inclusions of plagioclase, biotite, and quartz suggest that melting took place by the reaction

$$\text{Bt} + \text{Pl} + \text{Qtz} + \text{Fluid} = \text{Hbl} + \text{Granitic melt}. \quad (1)$$

Our interpreted melting reaction is comparable with that suggested by Timmermann *et al.* (2002), who proposed fluid-absent biotite-dehydration melting according to the reaction

$$\text{Bt} + \text{Pl} + \text{Qtz} = \text{Hbl} + \text{Granitic melt}. \quad (2)$$

Our reasons for invoking fluid-present partial melting, and the constraints on fluid composition, are explained below. In the following discussion, the term 'fluid' is used to describe a volatile phase (e.g. H_2O), whereas 'melt' is used to describe silicate melt ± entrained crystals.

Petrographic evidence suggests that partial melting in both stromatic and patch migmatite was associated with growth of new hornblende. Experimental studies

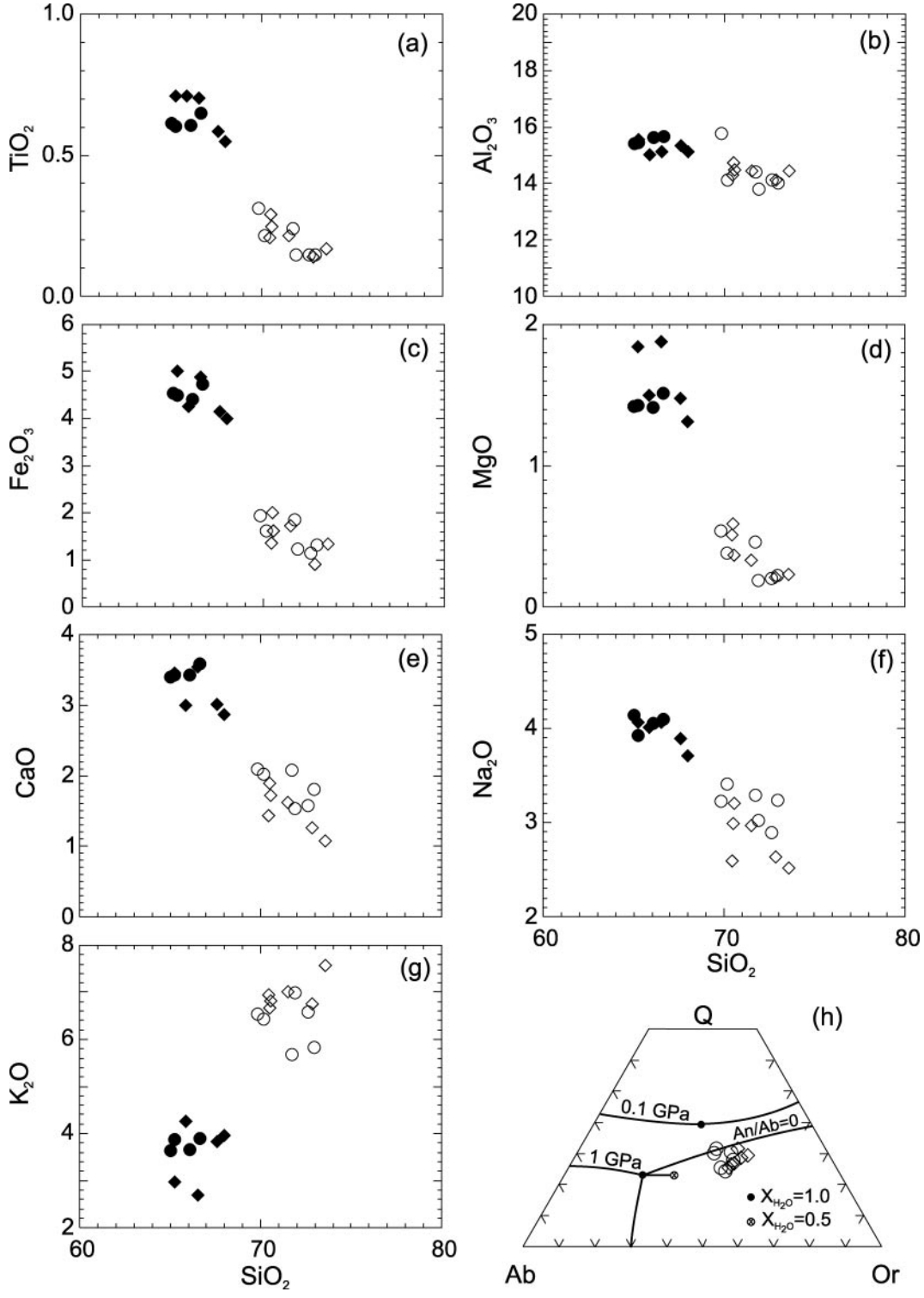

Fig. 9. Harker variation diagrams and normative Q–Ab–Or ternary diagram, showing the compositions of stromatic migmatites. For granodioritic mesosome: ●, Parkersville outcrop; ◆, Wren Lake outcrop; for concordant leucosome: ○, Parkersville outcrop; ◇, Wren Lake outcrop.

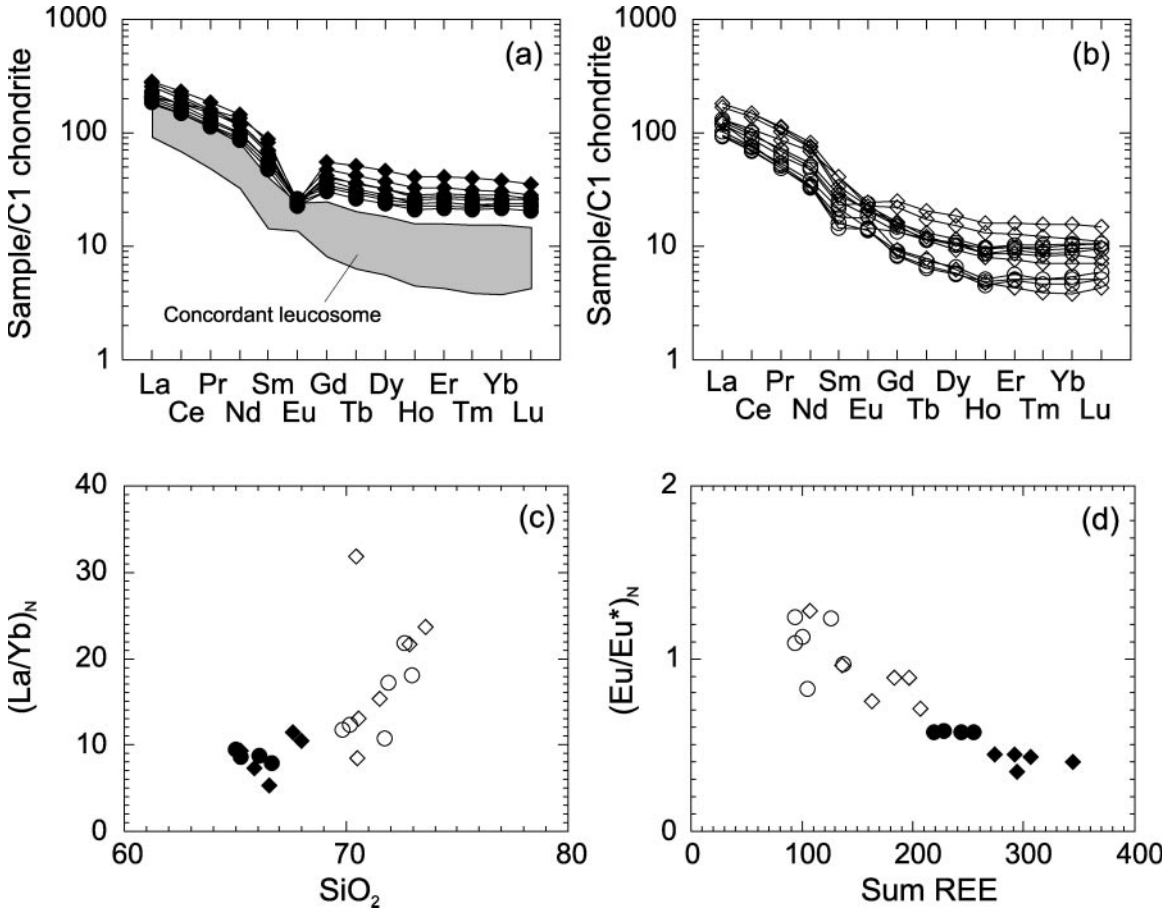

Fig. 10. Chondrite-normalized REE patterns for the stromatic migmatites comparing the various migmatite components, and bivariate trace element diagrams. Normalized to values of Sun & McDonough (1989). Symbols as in Fig. 9.

(e.g. Büsch *et al.*, 1974; Naney, 1983; Gardien *et al.*, 2000) have shown that crystallization and growth of hornblende during partial melting of a biotite–plagioclase–quartz assemblage requires at least 3–4 wt % H_2O in the melt. New hornblende can form by biotite-dehydration melting under fluid-absent conditions (e.g. Skjerlie & Johnston, 1996); however, in this case, the breakdown of biotite to form hornblende produces <5 vol. % melt at 850°C. Larger volumes of melt are produced at higher temperatures (>900°C), where hornblende reacts to form melt and residual pyroxene (e.g. Wolf & Wyllie, 1994); however, this reaction is not consistent with observations from the Muskoka migmatites.

If the granodioritic and dioritic mesosomes in the Muskoka migmatites represent the protoliths of the concordant and patch leucosomes, respectively, the relatively low abundance of biotite (<10 vol. %) is insufficient to produce significant melt volumes. For example, given 10 vol. % biotite with 3·9 wt % H_2O, and reasonable estimates of density (3·0 for biotite; 2·7 for source rock), up to 0·4 wt % H_2O is released by biotite breakdown. According to Clemens & Vielzeuf (1987), this amount of H_2O can produce *c.* 10 vol. % melt in a quartzofeldspathic source rock at 1 GPa. This is an upper estimate because the calculation assumes that all the fluid liberated by dehydration enters the melt (i.e. the residue is anhydrous); in contrast, partial melting in the Muskoka domain involved growth of a new hydrous phase (hornblende) that would have reduced the amount of fluid available to the melt. The estimated 10% melting is significantly less than the degree of partial melting estimated from the geochemical data (discussed below), thus fluid-absent, biotite-dehydration melting appears unlikely to have produced large amounts of melt in the Muskoka domain. Therefore, although small amounts of melt are likely to have formed by dehydration melting of biotite at T >800°C, we conclude that partial melting dominantly took place in the presence of an H_2O-bearing fluid

[reactions (3b) and (6c) in Fig. 3]. A similar model was invoked by McMullen (1999) for the eastern Muskoka domain, and has been proposed to account for partial melting of similar lithologies elsewhere (e.g. Lappin & Hollister, 1980; Kenah & Hollister, 1983; McLellan, 1988; Mogk, 1992; Nédélec *et al.*, 1993; Sawyer, 1998; Escuder Viruete, 1999).

The composition of the fluid is impossible to constrain without isotopic and/or fluid inclusion data. Phase equilibrium evidence from high-grade metamorphic rocks suggests that pure aqueous fluids are generally not present in excess [see Stevens & Clemens (1993) and references therein], thus, $a\mathrm{H_2O}$ was probably less than unity during migmatization. This is also consistent with the lack of leucosome in metabasite enclaves in the area [reaction (9) in Fig. 3]. Values of $a\mathrm{H_2O} < 1{\cdot}0$ can be achieved in systems that contain insufficient $\mathrm{H_2O}$-rich fluid to saturate the melt, or that contain a mixed-volatile fluid (e.g. $\mathrm{H_2O} + \mathrm{CO_2}$) (Clemens & Watkins, 2001). In the Muskoka domain, several observations suggest the presence of a mixed $\mathrm{H_2O} + \mathrm{CO_2}$ fluid during melting. The migmatites locally contain small amounts of carbonate associated with skeletal biotite and biotite–hornblende intergrowths that are interpreted to have been involved in melting (Fig. 6c). Diffuse granulite patches, also containing small amounts of carbonate (T. Slagstad, unpublished data, 2002), are common in parts of the Muskoka domain, and were interpreted by Timmermann *et al.* (2002) to have formed by influx of low-$a\mathrm{H_2O}$, $\mathrm{CO_2}$-rich fluids coeval with formation of the migmatites. Infiltration of $\mathrm{CO_2}$-rich fluid was also invoked by Pattison (1991) to explain the development of light-coloured 'net veins' rich in pyroxene, plagioclase, and locally quartz, in metagabbro enclaves in the adjacent Seguin subdomain (Fig. 2). Garnet porphyroblasts in pelitic gneisses in the underlying Algonquin domain (Fig. 2; north of Dorset) contain $\mathrm{CO_2}$-rich fluid inclusions interpreted to have formed as the result of partitioning of $\mathrm{H_2O}$ into coexisting melt (Layman, 2003).

We speculate that influx of a mixed $\mathrm{H_2O}$–$\mathrm{CO_2}$ fluid during high-grade Grenvillian metamorphism can account for both extensive partial melting (e.g. Giorgetti *et al.*, 1996) and the local development of granulite-facies assemblages. According to this model, $\mathrm{H_2O}$ would have been partitioned into the melts, whereas most of the $\mathrm{CO_2}$ would have remained in the rocks (see Clemens, 1993), forming the patch granulites and small accumulations of carbonate. During cooling and melt crystallization, back-reaction between $\mathrm{H_2O}$ and orthopyroxene could have formed the hornblende-rimmed orthopyroxenes typical of the patch granulites (Timmermann *et al.*, 2002). Detailed isotopic and fluid inclusion analyses from both the migmatites and the patch granulites are needed to determine the role and nature of fluids during high-grade metamorphism in these rocks.

Petrogenetic constraints from field and petrographic data

The field and petrographic observations from the patch migmatites provide important clues to their petrogenesis. The patch leucosomes are irregular, randomly distributed, and have associated melanosomes, consistent with *in situ* partial melting of dioritic mesosome (see McLellan, 1988). The partial melting reaction apparently produced a solid residue comprising 60–70 vol. % hornblende and 30–40 vol. % plagioclase as indicated by the petrographic observations. In addition, both patch and concordant melanosomes contain a significant proportion of biotite that we interpret to have formed during melt crystallization.

Thin seams of granitic material typically connect the patches and dykes and could represent former melt conduits along which granitic melts migrated from the patches. If this is true, the patch leucosomes may represent feldspar-rich cumulates, probably with some trapped, evolved melt. Melt migration probably took place by porous flow over distances of a few centimetres from melanosome to patch, and by channelled flow over distances of up to a few metres from patch to dyke. The zoning in the dykes, with feldspar-rich rims and quartz-rich centres, is similar to that observed in many granite–pegmatite systems (e.g. Jahns & Burnham, 1969; Simmons *et al.*, 1987), suggesting that feldspar crystallized from the melts. The pegmatitic texture indicates that the melts were water rich, and the network of granitic seams and pegmatite dykes could indicate that the magma and/or fluid pressure was great enough to cause fracturing of the host rock (e.g. Clemens & Mawer, 1992). Fluid-present melting is associated with a negative volume change, thus hydraulic fracturing is unlikely to have taken place during partial melting of the rocks. A more likely hypothesis, based on evidence for crystallization of hydrous melts (discussed further below), is that the magma reached water saturation, resulting in the formation of a free fluid phase, and thus a positive volume change, which caused fracturing of the surrounding rocks. Clear evidence of hydraulic fracturing (see Davidson *et al.*, 1994) is, however, missing from these rocks, and the process is considered only in passing in the petrogenetic model outlined below.

The high strain in the stromatic migmatites obscures many field and petrographic clues to their petrogenesis. Locally, however, the stromatic migmatites preserve features suggesting a comparable evolution to the patch migmatites. Irregularly distributed, thin melanosomes are common, suggesting that partial melting produced a hornblende + plagioclase-dominated residue like that associated with the patch migmatites. Coarse hornblende crystals, similar to the poikiloblastic hornblende in the patch migmatites, are locally present. Cross-cutting

leucosome dykes are relatively common (Fig. 5d) and may have formed by hydraulic fracturing during melt crystallization, as proposed for the patch migmatites.

Petrogenetic constraints of patch migmatites from trace element (REE) modelling

Partial melting

Trace element concentrations of model melts were calculated assuming equilibrium batch melting, in which the melt continually reacts and re-equilibrates with the solid residue at the site of melting until it is able to escape as a single 'batch'. The concentration of trace element i in the model melt ($C^i_{\rm L}$) is given by the equation

$$C^i_{\rm L} = \frac{C^i_0}{D^i_{\rm RS} + F(1 - D^i_{\rm RS})} \quad (3)$$

(Shaw, 1970), where $D^i_{\rm RS} = \sum D^i_a X_{\rm RS}$; $D^i_{\rm RS}$ is the bulk partition coefficient of element i in the residual solid, D^i_a is the partition coefficient of element i between melt and mineral a, $X_{\rm RS}$ is the weight proportion of mineral a in the residual solid, C^i_0 is the concentration of element i in the original solid, and F is the degree of partial melting. The concentration of element i in the complementary residue ($D^i_{\rm RS}$) is obtained by mass balance, such that

$$C^i_{\rm RS} = \frac{C^i_0 - FC^i_{\rm L}}{1 - F}. \quad (4)$$

Crystallization

The trace element distribution during melt crystallization is modelled assuming equilibrium crystallization, meaning that the crystallized solids (cumulate phases) remain in equilibrium with the melt throughout its crystallization history. We prefer the equilibrium crystallization model over the Rayleigh fractional crystallization model, in which only the crystal surfaces are in equilibrium with the melt, because a wealth of metamorphic, textural, and geochronological data from the Central Gneiss Belt (Culshaw *et al.*, 1997; Wodicka *et al.*, 2000) suggest protracted high-grade metamorphic conditions and slow regional cooling, which would have facilitated equilibration between melt and cumulate phases (e.g. Sawyer, 1987).

The concentration of trace element i in the evolved melt ($C^i_{\rm Lm}$) is given by the equation

$$C^i_{\rm Lm} = \frac{C^i_{\rm L0}}{F + D^i_{\rm CP}(1 - F)} \quad (5)$$

(Allègre & Minster, 1978; Hanson, 1978), where $D^i_{\rm CP} = \sum D^i_a X_{\rm CP}$; $D^i_{\rm CP}$ is the bulk partition coefficient of element i in the phases crystallized, D^i_a is the partition coefficient of element i between melt and mineral a, $X_{\rm CP}$ is the weight proportion of mineral a crystallized, $C^i_{\rm L0}$ is the concentration of element i in the primary melt, and F is the fraction of melt remaining. The concentration of element i in the complementary cumulate ($C^i_{\rm CP}$) is obtained by mass balance, such that

$$C^i_{\rm CP} = \frac{C^i_{\rm L0} - FC^i_{\rm Lm}}{1 - F}. \quad (6)$$

The trace element modelling is performed in two stages. Stage 1 models partial melting of the dioritic mesosome leaving a hornblende + plagioclase-dominated residue, producing a 'primary' melt (20–40% melting). Stage 2 models feldspar-dominated equilibrium crystallization in the patches. Partition coefficients and sources are given in Table 4.

As is nearly always the case with trace element modelling, the models are not unique, and several alternative models involving different phase proportions are possible. Here, we use the petrographic data to constrain the phase proportions in the models. This approach effectively tests whether the petrogenetic model devised from the petrographic data is consistent with the observed geochemistry of the rocks. Another well-known problem in applying trace element modelling to granitic (*sensu lato*) melts is the common presence of accessory phases such as apatite, zircon, allanite, and monazite. These phases are extremely rich in certain trace elements [e.g. light REE (LREE) in allanite and monazite, heavy REE (HREE) in zircon] and in many cases can obscure the effects produced by the major phases during partial melting and crystallization (e.g. Bea, 1996, and references therein). Zircon, apatite, and allanite are common accessory phases in the rocks studied here, particularly in the melanosomes, and therefore should be included in the models. Apatite has only moderate partition coefficients and does not differentiate the REE significantly, whereas zircon and allanite strongly fractionate the HREE and LREE, respectively. The partition coefficient for Eu in allanite is an order of magnitude smaller than that of the other middle REE (MREE) (Table 4); thus, fractionation of allanite influences the Eu anomaly in addition to the LREE. The effects of the accessory phases on the model results presented here are discussed in detail in the next section.

Stage 1: equilibrium melting of dioritic mesosome

The first stage of the model involves 20–40% equilibrium batch melting of the average dioritic mesosome. The model restite is hornblende dominated, as indicated by the petrographic data, comprising 63 wt % hornblende and 36 wt % plagioclase, with trace amounts of zircon, apatite, and allanite (see Fig. 11a and caption for details). The model melts are depleted in REE relative to the

Table 4: Partition coefficients used in partial melting modelling

	Plagioclase	K-feldspar	Hornblende	Biotite	Apatite	Allanite	Zircon
La	0·26	n.d.	0·74*	0·32*	20*	960	n.d.
Ce	0·24	0·044	1·52	0·32	34·7	940	2·64
Nd	0·17	0·025	4·26	0·29	57·1	750	2·2
Sm	0·13	0·018	7·77	0·26	62·8	620	3·14
Eu	0·814	1·13	5·14	0·24	30·4	56	3·14
Gd	0·09	0·011	10	0·28	56·3	440	12
Tb	0·09†	0·009†	12†	0·29†	54†	270	25†
Dy	0·086	0·006	13	0·29	50·7	200	45·7
Ho	0·085†	0·006†	12†	0·33†	45†	n.d.	100†
Er	0·084	0·006	12	0·35	37·2	100	135
Tm	0·08†	0·009†	10†	0·39†	30†	n.d.	200†
Yb	0·077	0·012	8·38	0·44	23·9	54	270
Lu	0·062	0·006	5·5	0·33	20	41	323

Data from Arth (1976) and Arth & Barker (1976), except *from Barbey *et al*. (1989) and †determined by extrapolation. Allanite data from Martin (1987), zircon data from Arth & Hanson (1975). n.d., no data.

source and have negligible Eu anomalies ($(Eu/Eu^*)_N$ = 0·91 and 0·87 for 20 and 40% partial melting, respectively), resembling the REE pattern for sample M30072-3-L2 with a $(Eu/Eu^*)_N$ of 0·89.

Apatite has a negligible impact on the model result; varying the amount of apatite in the residue from zero to 0·02 wt % produces a 15% variation in the total REE and <10% variation in the $(La/Yb)_N$ ratio. Apatite was, nevertheless, included because the petrographic data suggest that it is a common accessory phase. The geochemical data from the single patch melanosome analysis indicate *c.* 0·001 wt % apatite in the residue. Zircon effectively controls the amount of Tm, Yb, and Lu, and to a lesser extent Ho and Er, in the model melt; allanite controls the amount of the LREE and the size of the Eu anomaly. The proportion of zircon in the residue is estimated from the geochemical data to be *c.* 0·015 wt %. However, because zircon typically occurs as inclusions in refractory phases shielding it from the melt (e.g. Watson *et al.*, 1989) or because of limited solubility in the melt (e.g. Watson & Harrison, 1983), this is a maximum estimate of how much zircon participated in the melting reaction (e.g. Watson & Harrison, 1983; e.g. Watson *et al.*, 1989). Here, the proportions of zircon and allanite in the model residue were selected such that the REE pattern of the model melt resembled that observed for the patch leucosomes; that is, moderately negatively sloping LREE pattern and flat HREE pattern. The weight fraction of zircon participating in the melting reaction (0·0078 wt %) is about half that estimated from the geochemical data, suggesting that about half of the zircon present in the residue (patch melanosome) did not participate in the melting reaction. The amount of Zr in the leucosomes is relatively high, and calculations by Slagstad (2003) suggest that the melts were saturated in Zr. Thus, it is likely that limited solubility of Zr, possibly in addition to shielding by refractory phases, inhibited further dissolution of zircon. If the weight proportions of zircon and allanite participating in the melting reaction vary by >25% relative to those used in the partial melting model, the resulting model REE patterns (but not REE abundances) deviate significantly from the observed REE patterns of the patch leucosomes (Fig. 11b).

The REE contents of the model restite are similar to those of the patch melanosome, consistent with the latter representing the residue after melt extraction. The model melt produced by 40% partial melting was used as the 'primary' melt in stage 2.

Stage 2: crystallization in the patches

Stage 2 models equilibrium crystallization of the 'primary' melt produced in stage 1, crystallizing 60% K-feldspar, 20% plagioclase, and 20% quartz. The petrographic data suggest that K-feldspar is the main fractionating phase, but the K-feldspar/plagioclase ratio is unconstrained. Because both feldspars have small and essentially similar REE partition coefficients, changing the proportion of K-feldspar to plagioclase has a negligible effect on the model result. The interpretation that K-feldspar was a crystallizing phase implies that the partial melt generated in Stage 1 was relatively potassic. This is difficult to account for in the partial melting reaction proposed above, and it is possible that the infiltrating fluid introduced potassium to the melt system,

as observed in other migmatites (e.g. Olsen, 1984). In contrast, the solubility of REE in water-rich fluids is generally considered low, thus the REE contents of the patch migmatites were probably little affected by the infiltrating fluid. The results of the crystallization modelling suggest that most of the patch leucosomes and dykes are feldspar cumulates formed by extreme degrees of crystallization (95–99%). An alternative, and probably more realistic, interpretation is that the leucosomes and dykes represent cumulates, formed by lower degrees of crystallization than above, with some trapped evolved melt. Figure 11c shows the REE pattern obtained by mixing a cumulate derived by 40% crystallization with a varying weight fraction (0–50 wt %) of trapped, evolved melt. In this case, the majority of patch leucosomes and several of the dyke samples can be interpreted as cumulates mixed with 20–50 wt % evolved melt.

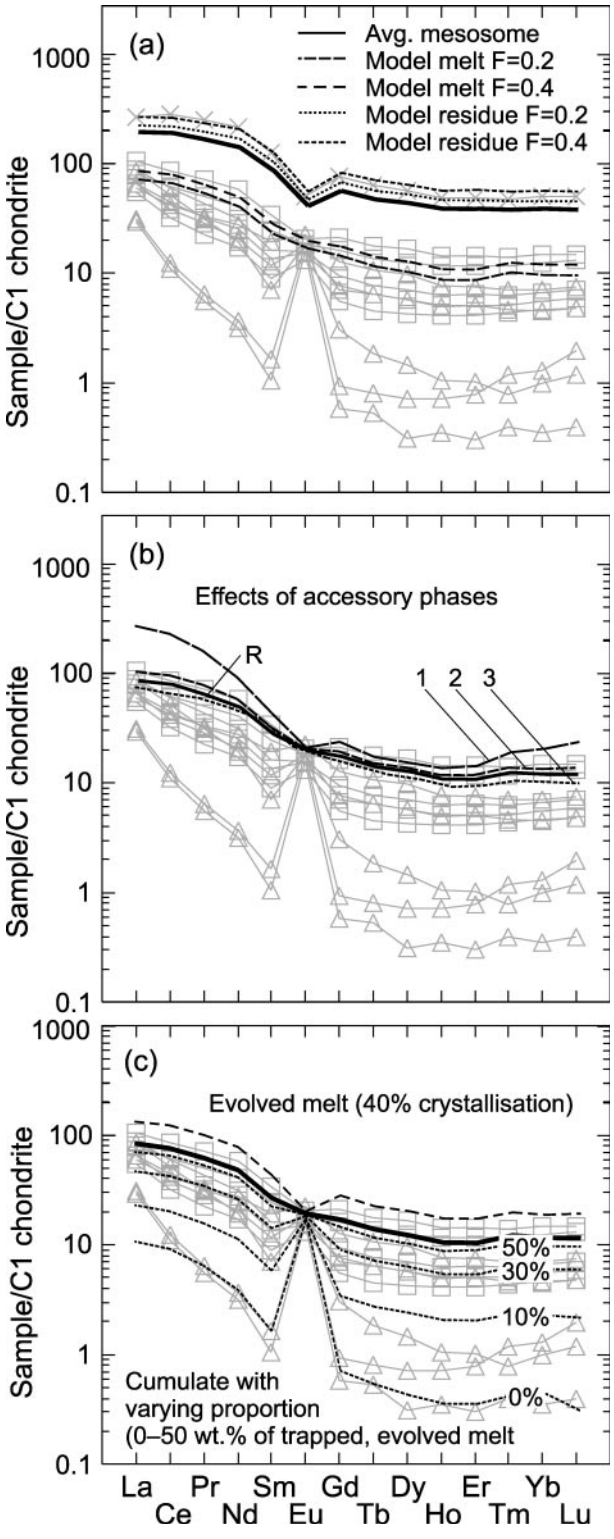

Fig. 11. Results of REE modelling on the patch migmatites using the equations presented in the text and partition coefficients from Table 4. (a) Partial melting of average dioritic mesosome (source) leaving a hornblende + plagioclase-dominated residue. Residue comprises (wt %) hornblende (63), plagioclase (36), zircon (0·0078), apatite (0·0053), and allanite (0·0027). Model melts and residues are calculated for 20 and 40% partial melting (i.e. $F = 0{\cdot}2$ and 0·4, respectively). Symbols as in Fig. 7. (b) Model melts formed by 40% partial melting, similar to (a), but with varying proportions of accessory phases. R, reference line 'Model melt $F = 0{\cdot}4$' in (a); 1, model melt with no accessory phases in the residue; 2, model melt with no apatite and −25% zircon (0·0059 wt %) and allanite (0·0020 wt %) relative to reference line (R); 3, model melt with 2 wt % apatite and +25% zircon (0·0096 wt %) and allanite (0·0034 wt %) relative to reference line (R). Reducing or increasing the proportions of allanite and zircon by more than 25% relative to the reference line yields model REE patterns that diverge significantly from those observed in the patch leucosomes. (c) Crystallization of a 'primary' melt produced by 40% partial melting in (a). Crystallizing phases are (in wt %) K-feldspar (60), plagioclase (20), and quartz (20). The modelling shows that the composition of the patch leucosomes and dykes is compatible with a cumulate, produced by 40% crystallization, mixed with various proportions (0–50 wt %) of evolved melt.

Petrogenesis of the stromatic migmatites

Despite the high strain, the stromatic migmatites preserve petrographic and geochemical features suggesting that they evolved in much the same way as the less deformed patch migmatites. In particular, the concordant leucosomes are rimmed by thin, discontinuous melanosomes with textures resembling those observed in the patch melanosomes. The observations are consistent with fluid-present melting of plagioclase, biotite, and quartz, leaving a hornblende + plagioclase-dominated residue, and producing a granitic melt. The REE patterns of the concordant leucosomes display a more positive Eu anomaly with decreasing total REE, similar to the patch leucosomes, indicating that feldspar-dominated crystallization was important in their evolution. In general, the concordant leucosomes have less positive Eu anomalies than the patch leucosomes. A likely explanation for this difference is that the granodioritic mesosome, a likely source composition for some of the concordant leucosomes, has a more negative Eu anomaly than the dioritic mesosome, which would result in a 'primary' melt with a

more negative Eu anomaly, assuming a similar melting reaction. Thus, despite their less positive Eu anomalies, we interpret the concordant leucosomes to represent crystal-rich melts or cumulates with some trapped, evolved melt; that is, similar to the patch leucosomes. This interpretation suggests that melts were continuously drained from the rocks, and may explain why the rocks did not develop into diatexites despite having present-day integrated leucosome proportions of up to 40–50 vol. % (see also Guernina & Sawyer, 2003).

The field, petrographic, and geochemical evidence from the stromatic migmatites suggests that in addition to *in situ* partial melting, a significant proportion of the leucosome present in the investigated outcrops was derived from external sources. There is no petrographic or geochemical evidence that the granodioritic mesosomes reported here (Table 1), or leucosome-poor grey gneisses throughout the Muskoka domain (Slagstad *et al.*, 2004*a*), are residual after large-scale melt extraction. This suggests that any externally derived melts must have migrated from structurally deeper, or more interior, parts of the orogen than those now exposed in the Muskoka domain, implying minimum melt transport distances of several kilometres.

MELT MIGRATION

Several mechanisms for melt transfer in the crust have been proposed, including diapirism (Bateman, 1984), dyking (Petford *et al.*, 1993*a*, 1993*b*), fracture propagation (Clemens & Mawer, 1992; Davidson *et al.*, 1994), and migration through faults or shear zones (Hollister & Crawford, 1986; Brown, 1994). In a study of the Mount Hay region of Australia, Collins & Sawyer (1996) proposed that melt migrated through a distributed, structurally controlled network of conduits developed during compressional, non-coaxial deformation. The driving force for melt transfer was interpreted to be fluid-pressure-driven dilatancy resulting from hydraulic fracturing, which formed a pervasive interconnected network through which the melts flowed. Although the geometry of the dykes in the patch migmatites is consistent with hydraulic fracturing, evidence of a similar process in the stromatic migmatites is less obvious. In these rocks fracturing may have been parallel to the foliation, controlled by the magnitude of difference in tensile strength normal and parallel to the schistosity, the orientation of the principal stress axes relative to the schistosity, and the differential stress applied to the rocks (see Wickham, 1987). However, local discordant, leucosome-filled veins in the stromatic migmatites (Fig. 5d) indicate that some steep fractures formed, possibly in structurally favourable sites or late in the deformation history.

Field observations from the stromatic migmatites suggest that melt was present during deformation, consistent with geochronological data (Timmermann *et al.*, 1997; Slagstad *et al.*, 2004*b*) showing that leucosomes formed at *c.* 1070–1050 Ma, during the main stage of the Ottawan orogeny. Based on the available data, we conclude that melt migration was driven by differential pressure associated with syn-melt deformation on the local to regional scale (see Sawyer, 1991, 1994; Brown, 1994; Collins & Sawyer, 1996). Melt transfer may have been dominantly vertical (towards the upper crust), with originally steep melt-transfer networks subsequently deformed into their present orientations, or melts may have migrated laterally along the sub-horizontal leucosome networks observed today. The prevalence of structures with low to moderate dips, even in relatively low-strain regions, is more consistent with the latter possibility. This implies lateral melt migration, and thus lateral pressure gradients, on a regional scale. If so, the Muskoka domain may represent the remnants of a regional-scale, melt-transfer zone developed at the mid-crustal level of an orogen large enough to have developed a significant differential pressure between its core and its flanks.

Despite indications that a large volume of melt migrated through the Muskoka domain, no map-scale Ottawan granite plutons that might correspond to melt collection zones have been identified in or near the study area. The absence of upper-crustal rocks in the Central Gneiss Belt means that the corresponding plutons, if they existed, may have been removed by erosion. This possibility is suggested by the abundance of Ottawan-age detrital zircons in Neoproterozoic sedimentary rocks from western North America (e.g. Ross *et al.*, 1992; Rainbird *et al.*, 1997) and in modern Appalachian rivers (Eriksson *et al.*, 2003).

CONCLUSIONS

(1) We recognize two distinct types of migmatite in the Muskoka domain, patch and stromatic migmatites, based on leucosome geometry and host-rock characteristics.

(2) The present-day morphology of migmatites in the Muskoka domain appears to be controlled by differences in strain. The geometry of leucosomes in the patch migmatites and the observation that deformed stromatic migmatites wrap around smaller, less deformed bodies of patch migmatite suggest that the dioritic rocks hosting the patch migmatites were stronger than the surrounding granodioritic orthogneisses, shielding the leucosomes from the effects of deformation.

(3) Both types of migmatite probably formed by fluid-present melting of plagioclase, biotite, and quartz, producing a hornblende + plagioclase-dominated residue and granitic melt. Crystallization of feldspar and quartz produced granitic cumulates, represented by most of the studied leucosomes. The fate of the complementary evolved melts could not be determined.

(4) Field and geochemical data from the stromatic migmatites suggest significant melt contributions from external sources, and indicate that the Muskoka domain may have acted as a mid-crustal melt transfer zone during Grenvillian (Ottawan) contractional deformation.

ACKNOWLEDGEMENTS

Barrie Clarke and Ed Sawyer provided very helpful comments on an earlier version of the paper, resulting in significant improvements. Pat Bogutyn provided able assistance in the field, and together with Kat Eisnor did much of the sample preparation. Gordon Brown made the thin sections. Pierre Barbey, Ed Sawyer, and Serge Fourcade are thanked for insightful reviews that improved and clarified the paper; Nick Arndt provided helpful editorial comments. T.S. was supported by a Dalhousie University Killam Scholarship and Ph.D. grant NFR-138552/432 from the Norwegian Research Council (NFR). Field and analytical work was funded by NSERC Discovery Grants to R.A.J. and N.G.C. Writing of this paper was carried out while T.S. was a post-doctoral fellow at the Geological Survey of Norway (NGU).

REFERENCES

Allègre, C. J. & Minster, J. F. (1978). Quantitative models of trace element behavior in magmatic processes. *Earth and Planetary Science Letters* **38**, 1–25.

Arth, J. G. (1976). Behaviour of trace elements during magmatic processes—a summary of theoretical models and their applications. *Journal of Research of the US Geological Survey* **4**, 41–47.

Arth, J. G. & Barker, F. (1976). Rare earth partitioning between hornblende and dacitic liquid and implications for the genesis of trondhjemitic–tonalitic magmas. *Geology* **4**, 534–536.

Arth, J. G. & Hanson, G. N. (1975). Geochemistry and origin of the early Precambrian crust of northeastern Minnesota. *Geochimica et Cosmochimica Acta* **39**, 325–362.

Ashworth, J. R. (1985). Introduction. In: Ashworth, J. R. (ed.) *Migmatites*. Glasgow: Blackie, pp. 1–35.

Barbey, P., Bertrand, J.-M., Angoua, S. & Dautel, D. (1989). Petrology and U/Pb geochronology of the Telohat migmatites, Aleksod, Central Hoggar, Algeria. *Contributions to Mineralogy and Petrology* **101**, 207–219.

Barraud, J., Gardien, V., Allemand, P. & Grandjean, P. (2004). Analogue models of melt-flow networks in folding migmatites. *Journal of Structural Geology* **26**, 307–324.

Bateman, R. (1984). On the role of diapirism in the segregation, ascent and final emplacement of granitoid magmas. *Tectonophysics* **110**, 211–231.

Bea, F. (1996). Residence of REE, Y, Th, and U in granites and crustal protoliths: implications for the chemistry of crustal melts. *Journal of Petrology* **37**, 521–552.

Beaumont, C., Jamieson, R. A., Nguyen, M. H. & Lee, B. (2001). Himalayan tectonics explained by extrusion of a low-viscosity crustal channel coupled to focused surface denudation. *Nature* **414**, 738–742.

Beaumont, C., Jamieson, R. A., Nguyen, M. H. & Medvedev, S. (2004). Crustal channel flows: 1. Numerical models with application to the tectonics of the Himalayan–Tibetan orogen. *Journal of Geophysical Research* **109**, B06406, doi: 10.1029/2003JB002809.

Brown, M. (1973). The definition of metatexis, diatexis and migmatite. *Proceedings of the Geologists' Association* **84**, 371–382.

Brown, M. (1979). The petrogenesis of the St. Malo migmatite belt, Armorican Massif, France, with particular reference to the diatexites. *Neues Jahrbuch für Mineralogie, Abhandlungen* **135**, 48–74.

Brown, M. (1994). The generation, segregation, ascent and emplacement of granite magma: the migmatite-to-crustally-derived granite connection in thickened orogens. *Earth-Science Reviews* **36**, 83–130.

Brown, M. & Solar, G. S. (1998). Granite ascent and emplacement during contractional deformation in convergent orogens. *Journal of Structural Geology* **20**, 1365–1393.

Brown, M., Averkin, Y. A., McLellan, E. L. & Sawyer, E. W. (1995). Melt segregation in migmatites. *Journal of Geophysical Research* **100**, 15655–15679.

Burr, J. L. & Carr, S. D. (1994). Structural geometry and U–Pb geochronology near Lithoprobe seismic Line 32, Western Central Metasedimentary Belt, Grenville Province, Ontario: new results from high precision U–Pb geochronology. In: Paper presented at Lithoprobe Abitibi–Grenville Project, Workshop Report, pp. 59–62.

Büsch, W., Schneider, G. & Mehnert, K. R. (1974). Initial melting at grain boundaries. Part II: melting in rocks of granodioritic, quartz dioritic, and tonalitic composition. *Neues Jahrbuch für Mineralogie, Monatshefte* **8**, 345–370.

Carr, S. D., Easton, R. M., Jamieson, R. A. & Culshaw, N. G. (2000). Geologic transect across the Grenville orogen of Ontario and New York. *Canadian Journal of Earth Sciences* **37**, 193–216.

Clemens, J. D. (1993). Experimental evidence against CO_2-promoted deep crustal melting. *Nature* **363**, 336–338.

Clemens, J. D. & Mawer, C. K. (1992). Granitic magma transport by fracture propagation. *Tectonophysics* **204**, 339–360.

Clemens, J. D. & Vielzeuf, D. (1987). Constraints on melting and magma production in the crust. *Earth and Planetary Science Letters* **86**, 287–306.

Clemens, J. D. & Watkins, J. M. (2001). The fluid regime of high-temperature metamorphism during granitoid magma genesis. *Contributions to Mineralogy and Petrology* **140**, 600–606.

Collins, W. J. & Sawyer, E. W. (1996). Pervasive granitoid magma transfer through the lower–middle crust during non-coaxial compressional deformation. *Journal of Metamorphic Geology* **14**, 565–579.

Conrad, W. K., Nicholls, I. A. & Wall, V. J. (1988). Water-saturated and -undersaturated melting of metaluminous and peraluminous crustal compositions at 10 kb: evidence for the origin of silicic magmas in the Taupo Volcanic Zone, New Zealand, and other occurrences. *Journal of Petrology* **29**, 765–803.

Culshaw, N. G. & Dostal, J. (1997). Sand Bay gneiss association, Grenville Province, Ontario: a Grenvillian rift- (and -drift) assemblage stranded in the Central Gneiss Belt? *Precambrian Research* **85**, 97–113.

Culshaw, N. G. & Dostal, J. (2002). Amphibolites of the Shawanaga domain, Central Gneiss Belt, Grenville Province, Ontario: tectonic setting and implications for relations between the Central Gneiss Belt and Midcontinental USA. *Precambrian Research* **113**, 65–85.

Culshaw, N. G., Davidson, A. & Nadeau, L. (1983). Structural subdivisions of the Grenville Province in the Parry Sound–Algonquin region, Ontario. *Current Research, Part B, Geological Survey of Canada, Paper* **83-1B**, 243–252.

Culshaw, N. G., Jamieson, R. A., Ketchum, J. W. F., Wodicka, N., Corrigan, D. & Reynolds, P. H. (1997). Transect across the

northwestern Grenville orogen, Georgian Bay, Ontario: polystage convergence and extension in the lower orogenic crust. *Tectonics* **16**, 966–982.

Davidson, A. (1984). Identification of ductile shear zones in the southwestern Grenville Province of the Canadian Shield. In: Kröner, A. & Greiling, E. (eds), *Precambrian Tectonics Illustrated*. Stuttgart: Schweizerbart, pp. 263–279.

Davidson, A. & van Breemen, O. (1988). Baddeleyite–zircon relationships in coronitic metagabbro, Grenville Province, Ontario: implications for geochronology. *Contributions to Mineralogy and Petrology* **100**, 291–299.

Davidson, C., Schmid, S. M. & Hollister, L. S. (1994). Role of melt during deformation in the deep crust. *Terra Nova* **6**, 133–142.

Dostal, J., Baragar, W. R. A. & Dupuy, C. (1986). Petrogenesis of the Natkusiak continental basalts, Victoria Island, Northwest Territories, Canada. *Canadian Journal of Earth Sciences* **23**, 622–632.

Eriksson, K. A., Campbell, I. H., Palin, M. & Allen, C. M. (2003). Predominance of Grenvillian magmatism recorded in detrital zircons from modern Appalachian rivers. *Journal of Geology* **111**, 707–717.

Escuder Viruete, J. (1999). Hornblende-bearing leucosome development during syn-orogenic crustal extension in the Tormes Gneiss Dome, NW Iberian Massif, Spain. *Lithos* **46**, 751–772.

Fyfe, W. S. (1973). The granulite facies, partial melting and the Archean crust. *Philosophical Transactions of the Royal Society of London, Series A* **273**, 457–461.

Gardien, V., Thompson, A. B. & Ulmer, P. (2000). Melting of biotite + plagioclase + quartz gneisses: the role of H_2O in the stability of amphibole. *Journal of Petrology* **41**, 651–666.

Giorgetti, G., Frezzotti, M.-L.-E., Palmeri, R. & Burke, E. A. J. (1996). Role of fluids in migmatites: CO_2–H_2O fluid inclusions in leucosomes from the Deep Freeze Range migmatites (Terra Nova Bay, Antarctica). *Journal of Metamorphic Geology* **14**, 307–317.

Green, A. G., Milkereit, B., Davidson, A., Spencer, C., Hutchinson, W. F., Cannon, W. F., Lee, M. W., Agena, W. F., Behrendt, J. C. & Hinze, W. J. (1988). Crustal structure of the Grenville Front and adjacent terranes. *Geology* **16**, 788–792.

Green, T. H. (1982). Anatexis of mafic crust and high pressure crystallization of andesite. In: Thorpe, R. S. (ed.) *Andesites*. London: John Wiley, pp. 465–487.

Guernina, S. & Sawyer, E. W. (2003). Large-scale melt-depletion in granulite terranes: an example from the Archean Ashuanipi Subprovince of Quebec. *Journal of Metamorphic Geology* **21**, 181–201.

Haggart, M. J., Jamieson, R. A., Reynolds, P. H., Krogh, T. E., Beaumont, C. & Culshaw, N. G. (1993). Last gasp of the Grenville orogeny—thermochronology of the Grenville Front Tectonic Zone near Killarney, Ontario. *Journal of Geology* **101**, 575–589.

Hanmer, S. & McEachern, S. J. (1992). Kinematical and rheological evolution of a crustal-scale ductile thrust zone, Central Metasedimentary Belt, Grenville orogen, Ontario. *Canadian Journal of Earth Sciences* **29**, 1779–1790.

Hanson, G. N. (1978). The application of trace elements to the petrogenesis of igneous rocks of granitic composition. *Earth and Planetary Science Letters* **38**, 26–43.

Hollister, L. S. (1993). The role of melt in the uplift and exhumation of orogenic belts. *Chemical Geology* **108**, 31–48.

Hollister, L. S. & Crawford, M. L. (1986). Melt-enhanced deformation: a major tectonic process. *Geology* **14**, 558–561.

Jahns, R. H. & Burnham, C. W. (1969). Experimental studies of pegmatite genesis: I. A model for the derivation and crystallization of granitic pegmatites. *Economic Geology* **64**, 843–864.

Jamieson, R. A., Beaumont, C., Nguyen, M. H. & Lee, B. (2002). Interaction of metamorphism, deformation and exhumation in large convergent orogens. *Journal of Metamorphic Geology* **20**, 9–24.

Johannes, W. & Holtz, F. (1990). Formation and composition of H_2O-undersaturated granitic melts. In: Ashworth, J. R. & Brown, M. (eds) *High-temperature Metamorphism and Crustal Anatexis*. *Mineralogical Society Series* **2**, 87–104.

Kenah, C. & Hollister, L. S. (1983). Anatexis in the Central Gneiss Complex, British Columbia. In: Atherton, M. P. & Gribble, C. D. (eds), *Migmatites, Melting and Metamorphism*. Nantwich: Shiva, pp. 142–162.

Ketchum, J. W. F., Heaman, L. M., Krogh, T. E., Culshaw, N. G. & Jamieson, R. A. (1998). Timing and thermal influence of late orogenic extension in the lower crust: a U–Pb geochronological study from the southwest Grenville orogen, Canada. *Precambrian Research* **89**, 25–45.

Kretz, R. (1983). Symbols for rock-forming minerals. *American Mineralogist* **68**, 277–279.

Krogh, T. E. (1994). Precise U–Pb ages for Grenvillian and pre-Grenvillian thrusting of Proterozoic and Archean metamorphic assemblages in the Grenville Front Tectonic Zone, Canada. *Tectonics* **13**, 963–982.

Lappin, A. R. & Hollister, L. S. (1980). Partial melting in the Central Gneiss Complex near Prince Rupert, British Columbia. *American Journal of Science* **280**, 518–545.

Layman, A. J. (2003). Composition and significance of fluid inclusions in garnet, Algonquin Domain, Central Gneiss Belt, Grenville Province, Ontario. B.Sc.(Hons) thesis, Dalhousie University, Halifax.

Longerich, H. P., Jenner, G. A., Fryer, B. J. & Jackson, S. E. (1990). Inductively coupled plasma-mass spectrometric analysis of geological samples: a critical evaluation based on case studies. *Chemical Geology* **83**, 105–118.

Martin, H. (1987). Petrogenesis of Archean trondhjemites, tonalites, and granodiorites from eastern Finland: major and trace element geochemistry. *Journal of Petrology* **28**, 921–953.

McEachern, S. J. & van Breemen, O. (1993). Age of deformation within the Central Metasedimentary Belt boundary thrust zone, southwest Grenville orogen: constraints on the collision of the Mid-Proterozoic Elzevir terrane. *Canadian Journal of Earth Sciences* **30**, 1155–1165.

McLellan, E. L. (1988). Migmatite structures in the Central Gneiss Complex, Boca de Quadra, Alaska. *Journal of Metamorphic Geology* **6**, 517–542.

McMullen, S. M. (1999). Tectonic evolution of the Bark Lake area, eastern Central Gneiss Belt, Ontario Grenville: constraints from geology, geochemistry and U–Pb geochronology. M.Sc. thesis, Carleton University, 175 pp.

Mogk, D. W. (1992). Ductile shearing and migmatization at mid-crustal levels in an Archean high-grade gneiss belt, northern Gallatin Range, Montana, USA. *Journal of Metamorphic Geology* **10**, 427–438.

Montel, J. M., Marignac, C., Barbey, P. & Pichavant, M. (1992). Thermobarometry and granite genesis: the Hercynian low-*P*, high-*T* Velay anatectic dome (French Massif Central). *Journal of Metamorphic Geology* **10**, 1–15.

Moore, J. M. & Thompson, P. H. (1980). The Flinton group: a late Precambrian metasedimentary succession in the Grenville Province of eastern Ontario. *Canadian Journal of Earth Sciences* **17**, 1685–1707.

Nadeau, L. & van Breemen, O. (1998). Plutonic ages and tectonic setting of the Algonquin and Muskoka allochthons, Central Gneiss Belt, Grenville Province, Ontario. *Canadian Journal of Earth Sciences* **35**, 1423–1438.

Naney, M. T. (1983). Phase equilibria of rock-forming ferromagnesian silicates in granitic systems. *American Journal of Science* **238**, 993–1033.

Nédélec, A., Minyem, D. & Barbey, P. (1993). High-*P*–high-*T* anatexis of Archean tonalitic grey gneisses: the Eseka migmatites, Cameroon. *Precambrian Research* **62**, 191–205.

Olsen, S. N. (1984). Mass-balance and mass-transfer in migmatites from the Colorado Front Range. *Contributions to Mineralogy and Petrology* **85**, 30–44.

Patiño Douce, A. E. & Beard, J. S. (1995). Dehydration-melting of biotite gneiss and quartz amphibolite from 3 to 15 kbar. *Journal of Petrology* **36**, 707–738.

Pattison, D. R. M. (1991). Infiltration-driven dehydration and anatexis in granulite facies metagabbro, Grenville Province, Ontario, Canada. *Journal of Metamorphic Geology* **9**, 315–332.

Peterson, J. W. & Newton, R. C. (1989). Reversed experiments on biotite–quartz–feldspar melting in the system KMASH: implications for crustal anatexis. *Journal of Geology* **97**, 465–485.

Petford, N., Kerr, R. C. & Lister, J. R. (1993*a*). Dike transport of granitoid magmas. *Geology* **21**, 845–848.

Petford, N., Lister, J. R. & Kerr, R. C. (1993*b*). The ascent of felsic magmas in dykes. *Lithos* **32**, 161–168.

Rainbird, R. H., McNicoll, V. J., Thériault, R. J., Heaman, L. M., Abbott, J. G., Long, D. G. F. & Thorkelson, D. J. (1997). Pan-continental river system draining Grenville orogen recorded by U–Pb and Sm–Nd geochronology of Neoproterozoic quartzarenites and mudrocks, northwestern Canada. *Journal of Geology* **105**, 1–17.

Rivers, T. (1997). Lithotectonic elements of the Grenville Province: review and tectonic implications. *Precambrian Research* **86**, 117–154.

Rivers, T. & Corrigan, D. (2000). Convergent margin on southeastern Laurentia during the Mesoproterozoic: tectonic implications. *Canadian Journal of Earth Sciences* **37**, 359–383.

Robin, P.-Y. F. (1979). Theory of metamorphic segregation and related processes. *Geochimica et Cosmochimica Acta* **43**, 1587–1600.

Ross, G. M., Parrish, R. R. & Winston, D. (1992). Provenance and U–Pb geochronology of the Mesoproterozoic Belt Supergroup (northwestern United States): implications for the age of deposition and pre-Panthalassa plate reconstructions. *Earth and Planetary Science Letters* **113**, 57–76.

Rutter, M. J. & Wyllie, P. J. (1988). Melting of vapour-absent tonalite at 10 kbar to simulate dehydration-melting in the deep crust. *Nature* **331**, 159–160.

Sandiford, M. & McLaren, S. (2002). Tectonic feedback and the ordering of heat producing elements within the continental lithosphere. *Earth and Planetary Science Letters* **204**, 133–150.

Sawyer, E. W. (1987). The role of partial melting and fractional crystallization in determining discordant leucosome compositions. *Journal of Petrology* **28**, 445–473.

Sawyer, E. W. (1991). Disequilibrium melting and the rate of melt–residuum separation during migmatization of mafic rocks from the Grenville Front, Quebec. *Journal of Petrology* **32**, 701–738.

Sawyer, E. W. (1994). Melt segregation in the continental crust. *Geology* **22**, 1019–1022.

Sawyer, E. W. (1998). Formation and evolution of granite magmas during crustal reworking: the significance of diatexites. *Journal of Petrology* **39**, 1147–1167.

Sawyer, E. W. (1999). Criteria for the recognition of partial melting. *Physics and Chemistry of the Earth (A)* **24**, 269–279.

Sawyer, E. W. (2001). Melt segregation in the continental crust: distribution and movement of melt in anatectic rocks. *Journal of Metamorphic Geology* **19**, 291–309.

Sawyer, E. W., Dombrowski, C. & Collins, W. J. (1999). Movement of melt during synchronous regional deformation and granulite-facies anatexis, an example from the Wuluma Hills, central Australia. In: Castro, A., Fernandez, C. & Vigneresse, J. L. (eds) *Understanding Granites: Integrating New and Classical Techniques. Geological Society, London, Special Publications* **168**, 221–237.

Shaw, D. M. (1970). Trace element fractionation during anatexis. *Geochimica et Cosmochimica Acta* **34**, 237–243.

Simmons, W. B., Lee, M. T. & Brewster, R. H. (1987). Geochemistry and evolution of the South Platte granite–pegmatite system, Jefferson County, Colorado. *Geochimica et Cosmochimica Acta* **51**, 455–471.

Skjerlie, K. P. & Johnston, A. D. (1996). Vapour-absent melting from 10 to 20 kbar of crustal rocks that contain multiple hydrous phases: implications for anatexis in the deep to very deep continental crust and active continental margins. *Journal of Petrology* **37**, 661–691.

Slagstad, T. (2003). Muskoka and Shawanaga domains, Central Gneiss Belt, Grenville Province, Ontario: geochemical and geochronological constraints on pre-Grenvillian and Grenvillian geological evolution. Ph.D. thesis, Dalhousie University, Halifax.

Slagstad, T., Culshaw, N. G., Jamieson, R. A. & Ketchum, J. W. F. (2004*a*). Early Mesoproterozoic tectonic history of the southwestern Grenville Province, Ontario: constraints from geochemistry and geochronology of high-grade gneisses. In: Tollo, R. P., Corriveau, L., McLelland, J. & Bartholomew, M. J. (eds) *Proterozoic Tectonic Evolution of the Grenville Orogen in North America. Geological Society of America, Memoir* **197**, 209–241.

Slagstad, T., Hamilton, M. A., Jamieson, R. A. & Culshaw, N. G. (2004*b*). Timing and duration of melting in the mid orogenic crust: constraints from U–Pb (SHRIMP) data, Muskoka and Shawanaga domains, Grenville Province, Ontario. *Canadian Journal of Earth Sciences* **41**, 1339–1365.

Solar, G. S. & Brown, M. (2001). Petrogenesis of migmatites in Maine, USA: possible source of peraluminous leucogranite in plutons. *Journal of Petrology* **42**, 789–823.

Stevens, G. & Clemens, J. D. (1993). Fluid-absent melting and the roles of fluids in the lithosphere: a slanted summary? *Chemical Geology* **108**, 1–17.

Sun, S.-S. & McDonough, W. F. (1989). Chemical and isotopic systematics of oceanic basalts: implications for mantle composition and processes. In: Saunders, A. D. & Norry, M. J. (eds) *Magmatism in the Ocean Basins. Geological Society, London, Special Publications* **42**, 313–345.

Symmes, G. H. & Ferry, J. M. (1995). Metamorphism, fluid flow and partial melting in pelitic rocks from the Onawa contact aureole, central Maine, USA. *Journal of Petrology* **36**, 587–612.

Thompson, A. B. (1982). Dehydration melting of pelitic rocks and the generation of H_2O-undersaturated granitic liquids. *American Journal of Science* **282**, 1567–1595.

Timmermann, H. (1998). Geology, metamorphism, and U–Pb geochronology in the Central Gneiss Belt between Huntsville and Haliburton, southwestern Grenville Province, Ontario. Ph.D. thesis, Dalhousie University, Halifax, 410 pp.

Timmermann, H., Parrish, R. R., Jamieson, R. A. & Culshaw, N. G. (1997). Time of metamorphism beneath the Central Metasedimentary Belt boundary thrust zone, Grenville orogen, Ontario: accretion at 1080 Ma? *Canadian Journal of Earth Sciences* **34**, 1023–1029.

Timmermann, H., Jamieson, R. A., Parrish, R. R. & Culshaw, N. G. (2002). Coeval migmatites and granulites, Muskoka domain, southwestern Grenville Province. *Canadian Journal of Earth Sciences* **39**, 239–258.

van Breemen, O. & Hanmer, S. (1986). Zircon morphology and U–Pb geochronology in active shear zones: studies of syntectonic intrusions along the northwest boundary of the Central Metasedimentary Belt, Grenville Province, Ontario. *Current Research, Part B, Geological Survey of Canada, Paper* **86-1B**, 775–784.

van der Pluijm, B. A. & Carlson, K. A. (1989). Extension in the Central Metasedimentary Belt of the Ontario Grenville: timing and tectonic significance. *Geology* **17**, 161–164.

Vielzeuf, D., Clemens, J. D., Pin, C. & Moinet, E. (1990). Granites, granulites and crustal differentiation. In: Vielzeuf, D. & Vidal, P. (eds), *Granulites and Crustal Evolution*. Dordrecht: Kluwer Academic, pp. 551–568.

Waters, D. J. (2001). The significance of prograde and retrograde quartz-bearing intergrowth microstructures in partially melted granulite-facies rocks. *Lithos* **56**, 97–110.

Watson, E. B. & Harrison, T. M. (1983). Zircon saturation revisited: temperature and composition effects in a variety of crustal magma types. *Earth and Planetary Science Letters* **64**, 295–304.

Watson, E. B., Vicenzi, E. P. & Rapp, R. P. (1989). Inclusion/host relations involving accessory minerals in high-grade metamorphic and anatectic rocks. *Contributions to Mineralogy and Petrology* **101**, 220–231.

White, D. J., Easton, R. M., Culshaw, N. G., Milkereit, B., Forsyth, D. A., Carr, S. D., Green, A. G. & Davidson, A. (1994). Seismic images of the Grenville Orogen in Ontario. *Canadian Journal of Earth Sciences* **31**, 293–307.

Wickham, S. M. (1987). The segregation and emplacement of granitic magmas. *Journal of the Geological Society, London* **144**, 281–297.

Wodicka, N., Ketchum, J. W. F. & Jamieson, R. A. (2000). Grenvillian metamorphism of monocyclic rocks, Georgian Bay, Ontario, Canada: implications for convergence history. *Canadian Mineralogist* **38**, 471–510.

Wolf, M. B. & Wyllie, P. J. (1994). Dehydration-melting of amphibolite at 10 kbar: the effects of temperature and time. *Contributions to Mineralogy and Petrology* **115**, 369–383.

Wynne-Edwards, H. R. (1972). The Grenville Province. In: Price, R. A. & Douglas, R. J. W. (eds) *Variations in Tectonic Styles in Canada. Geological Association of Canada Special Paper* **11**, 263–334.